Hardware for Studying Aurora

Lillia Hammond

Advisor: Professor Kristina Lynch, Professor David Hanneke
May 8, 2025

Submitted to the
Department of Physics & Astronomy of Amherst College
in partial fulfilment of the
requirements for the degree of
Bachelors of Arts with honors

© 2025 Lillia Hammond

Abstract

The aurora borealis is a visible phenomenon that occurs in our atmosphere at high latitudes. The aurora occurs when energized electrons strike the neutral atmosphere and make the molecules glow. The shape of the aurora is determined by the ionosphere's coupling to the magnetosphere, Earth's magnetic field. The 317 Rocket Lab's goal is to study aurora to gain a stronger understanding of the ionosphere's structure.

One method of gathering in situ data at our target altitude (150-500 km) is with sounding rockets. These are small, relatively affordable rockets which house scientific instrumentation in their payloads to collect data. Our current sounding rocket mission, the GNEISS (Geophysical Non-Equilibrium Ionospheric System Science) mission, aims to study spatial and temporal variations along auroral arcs to further understand the ionosphere's structure. We will collect this data by sending two identical, near-simultaneous sounding rockets through two different slices of the same auroral arc. Analyzing the difference in the ionospheric parameters on these two trajectories through the aurora will fill gaps in our understanding of variations along aurora which have not previously been studied. Launching near-simultaneous rockets is rare. Moreover, this sounding rocket mission will be the first to launch two rockets within a two-minute window with azimuthal separation.

For my thesis, I have designed and updated a family of flight hardware to collect in situ auroral data. I made significant mechanical improvements and fabrication process changes to our Petite Ion Probes (PIPs) which collect ionospheric data. These PIPs reside on the main sounding rocket payloads and on ejectable subpayloads, called Bobs, which I have also improved. In addition, I have made new complementary structural supports for the PIPs, called PIP trees, and new electronics housing boxes, the shield board box and the Lattice box, for the GNEISS sounding rockets. Each of these designs was constrained by the sounding rocket environment, the instrument's requirements, and manufacturing limitations.

These changes will improve the manufacturing process while maintaining, and potentially improving, the quality of data acquisition for the GNEISS rocket mission. Therefore, it will contribute to our understanding of the ionosphere's structure. Additionally, these improvements may inform the hardware design of future sounding rocket missions, aurora focused or otherwise.

Acknowledgments

I would like to thank Prof. Kristina Lynch for her guidance throughout my thesis project. I have learned so much from you over the last two years. I am very grateful for the time you gave put into integrating me into the lab.

I would also like to thank the rest of the 317 Rocket Lab at Dartmouth College. I would like to specifically thank Jeff Renk for his support with hardware electronics, Alan Goldblatt and Rowan Kowalsky for their work on the screen fabrication, and our graduate students, Alexander Mule, Jules van Irsel, and Magdalina Moses, for their support. I would like to thank the other undergraduates in the 317 Rocket Lab, especially Sean Wallace for all of his help gathering photos of hardware. Writing a remote thesis is not easy, but the incredibly fascinating work we do made it such a worthwhile experience. I am excited to continue working with you all when I return to the lab next year in person.

I would also like to acknowledge Kye Cooley and Chris Grant, the machinists I work with at Dartmouth College. Thank you for working with me to improve the manufacturing process for the GNEISS mission.

Thank you to Darren Nichols, Josh Yacobucci, and Philip Cathel, our NSROC engineering team, for maintaining constant lines of communication and collaborating with me throughout this project.

This thesis would not have been possible without Prof. David Hanneke, my thesis advisor here at Amherst. Navigating a remote thesis was not a simple task, but your guidance and support allowed me to carry out this thesis.

Thank you to Jim Kubasek for teaching me everything I know about precision machining and modeling in CAD. Working on projects in the machine shop throughout my time at Amherst has been an incredibly meaningful experience and has absolutely influenced my path to this thesis project.

Thank you to my parents, grandparents, brother, and friends for supporting me throughout my thesis. Finally, I would like to thank my teammates in Amherst Club Volleyball for always providing me with an outlet outside of my thesis work.

This work would not have been possible without funding from NASA NH Space Grant, NASA EPSCoR, and NASA LCAS GNEISS.

Contents

List of Figures

Chapter 1

Introduction

1.1 Aurora Borealis

The phenomenon of the aurora borealis begins at the Sun. Charged particles in the Sun, mainly hydrogen ions, helium ions, and electrons, are expelled from the Sun's surface as they begin their journey outward into space. This is the solar wind [1]. There are charged particles, aside from the solar wind, that orbit the Sun. These particles compose the solar equatorial current, a sheet current which orbits the Sun at its equator. In general, the solar wind does not contribute to the solar equatorial current. Because positively and negatively charged particles travel together in the solar wind's plasma, it results in no net current.

1.1.1 Interplanetary Magnetic Field

The Interplanetary Magnetic Field (IMF) is a result of the solar equatorial current, as shown in Figure 1.1 [1]. Using Ampere's Law, the total current through a loop is proportional to the magnetic field around the loop [2].

$$\oint_C \boldsymbol{B} \cdot \boldsymbol{d\ell} = \mu_0 I_C \tag{1.1}$$

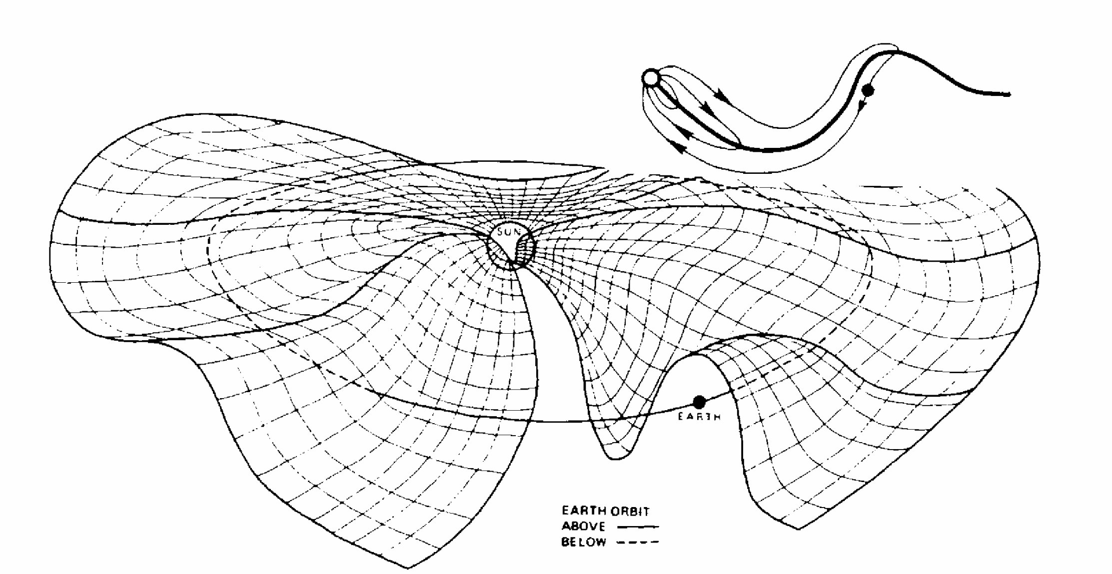

Figure 1.1: Solar equatorial current and Interplanetary Magnetic Field. Plasma from the Sun composes the solar equatorial current which orbits the Sun. The solar equatorial current is described by the circular lines on the current sheet. On the top right, a secondary image shows the current sheet directed into the page which results in looped magnetic field lines, otherwise known as the Interplanetary Magnetic Field. One of these field lines intersects the Earth and is able to interact with the magnetosphere. Reprinted from The Earth's Ionosphere, Vol 1, Michael C. Kelley, Introductory and Background Material, 16, 1989, with permission from Elsevier.

As shown in the upper right drawing of Figure 1.1, the equatorial sheet current will result in a magnetic field. The solar equatorial current travels counterclockwise around the Sun at the Sun's equator, as shown in Figure 1.1. However, the sheet current does not form a flat disc. Instead, it forms folds and curves, similar to a flowing skirt. When the sheet current forms these curves, the IMF will mimic the geometry, as magnetic fields are perpendicular to their corresponding sheet currents [2]. The direction of the curve of the solar equatorial current is random at the location of Earth. Therefore, the vertical component of the IMF at Earth is random at a given time.

1.1.2 Magnetosphere

A portion of the ions and electrons ejected from the Sun continuously bring momentum and energy to Earth. We on Earth are significantly protected from particles of the solar wind by Earth's magnetic field, called the magnetosphere. The magnetosphere, which has a dipole shape, guides the potentially harmful particles towards the magnetic poles.

The solar wind affects the shape of Earth's magnetosphere. The solar wind exerts pressure on the magnetic field which compresses the side of the magnetosphere near the Sun, the dayside, and stretches the magnetosphere on the side far from the Sun, the nightside [3]. This causes the magnetosphere to not be a perfect dipole as seen in Figure 1.2.

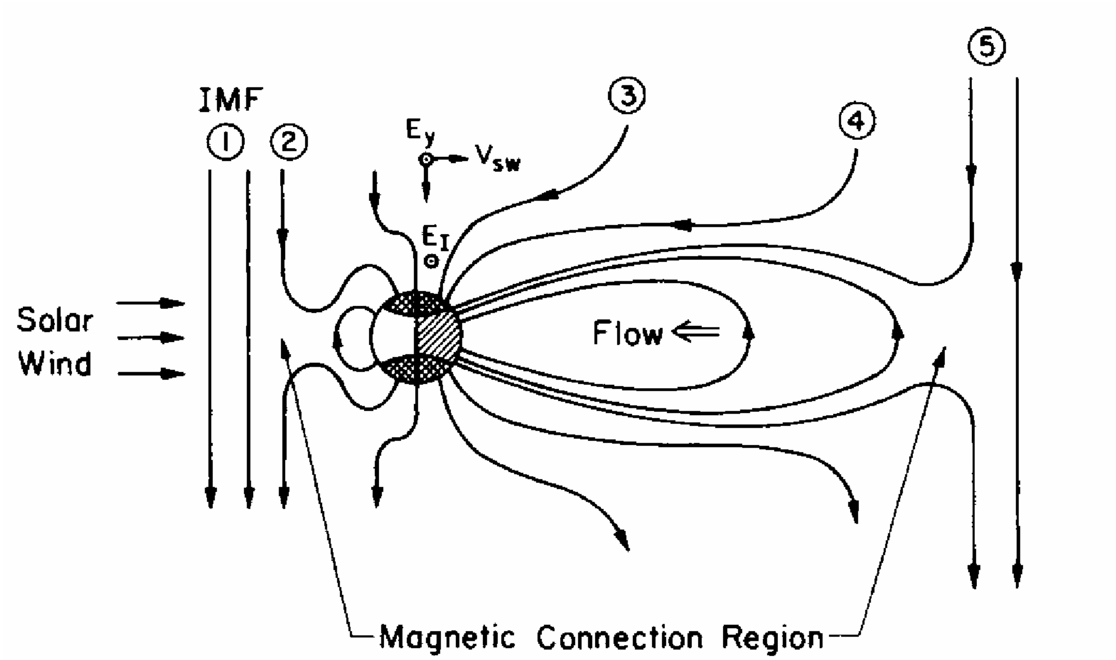

Figure 1.2: Earth's magnetosphere. The compressed dayside and elongated nightside magnetic fields are due to the solar wind. When the IMF has a southward vertical component, both the dayside and nightside of the magnetosphere experience reconnection which allows particles from the Sun to travel towards Earth's atmosphere. The numbers 1-5 differentiate the various IMF lines. IMF line 2 shows dayside reconnection, and IMF line 5 shows nightside reconnection. Reprinted from The Earth's Ionosphere, Vol 1, Michael C. Kelley, Introductory and Background Material, 19, 1989, with permission from Elsevier.

That said, the magnetosphere still maintains its positive and negative poles and general dipole shape. There are still magnetic field lines leaving the geographic south and pointing northward. Therefore, the general vertical component of the magnetic field is northward along the magnetosphere equator.

At Earth, the vertical component of the IMF will either be positive (northward) or a negative (southward) depending on the the solar equatorial current. At a given moment, the direction is random. The IMF will superimpose itself onto the Earth's magnetosphere. If the IMF has a positive (northward) component, both magnetic fields will be in the same direction, and coupling between the two regions is minimized. However, if the IMF has a negative (southward) component, it will experience reconnection with the magnetosphere's positive component. Reconnection is demonstrated by IMF lines 2 and 5 in Figure 1.2. Particles that originally traveled along either the IMF or magnetosphere field lines will instead change tracks onto their reconnected path. This allows particles from the Sun to enter the magnetosphere and become magnetospheric particles [4].

1.1.3 The Snap

The first instance of reconnection happens on the dayside, as shown with IMF line 2 in Figure 1.2. This can result in dayside aurora [5]. As the reconnected magnetic field lines from the IMF appear to move away from the Sun, they will appear to wrap around the Earth, beginning to collapse on the nightside as a result of reconnection. For a second time, now on the nightside, this reconnection process allows particles to switch paths from IMF lines onto magnetosphere field lines as seen with IMF line 5 in Figure 1.2 [3][4].

Another way to think about this process of reconnection is in terms of energy. As the solar wind propagates into space, it directs energy towards Earth which is absorbed by the Earth's magnetic field. At a certain point, too much energy is added to the magnetic field which causes the nightside magnetic field to be distorted tailward (away from the Sun) until it snaps back. This is similar to a water droplet dripping from a faucet. As more water is added to the droplet, it begins to stretch out and eventually breaks off as a water drop. The remaining water snaps back because of water tension.[1]

After reconnection on the nightside, the particles originating from the solar wind have become nightside tail particles. A potential drop encourages nightside tail electrons to accelerate towards Earth. This is a consequence of magnetosphere forming an imperfect dipole. Because the dipole is not ideal, the curl of the magnetosphere will be nonzero. When inspecting the Ampere-Maxwell Law, it becomes clear that there must be some $\boldsymbol{J}$ which satisfies the equation for some nonzero $\nabla \times \boldsymbol{B}$ and a corresponding voltage drop which prompts this current[2] [2].

$$\nabla \times \boldsymbol{B} = \mu_0 \varepsilon_0 \frac{d\boldsymbol{E}}{dt} + \mu_0 \boldsymbol{J} \tag{1.2}$$

The accelerating potential drop directs electrons towards the Earth. These electrons rapidly spiral along the magnetic field lines as they are driven into the atmosphere. This is described by the Lorentz force [2].

$$\boldsymbol{F} = q(\boldsymbol{E} + \boldsymbol{v} \times \boldsymbol{B}) \tag{1.3}$$

An electron's component of velocity perpendicular to the magnetic field will cause it to rapidly precess around it. This is cyclotron motion. Each electron will move around a magnetic field line while traveling down the field towards Earth. Much like a hose spraying into a pond, these electrons are accelerated into the lower ionosphere. As the particles are driven towards Earth, they will collide with molecules in the atmosphere, such as oxygen and nitrogen. Exciting these molecules emits light.

Given the geometry of the magnetosphere, the particles originating from the solar wind will be driven into Earth at a certain latitude depending on the strength of the solar wind.

[1] This snap is the reconnection. Treating the aurora like a continuous fluid, like in this example of a water droplet, is a fair approximation at large scales. The comparison only begins to break down at smaller scales when the charge of the individual motion of charged particles in the plasma begins to play a larger role in its movement.

[2] We can assume there is no displacement current because we are operating in a static model.

Figure 1.3: Aurora borealis in rural Alaska. Photo courtesy of Alexander Mule.

The latitude corresponding to the transition between the magnetosphere's open and closed field lines is where the auroral ovals exist. Magnetic field lines at this latitude are the first to experience reconnection. Therefore, the particles traveling along the IMF will have their first opportunity to switch paths onto a magnetosphere field line at this location. This is why the aurora can only be seen at certain latitudes in the northern and southern hemispheres. The aurora will nominally appear to be a uniform arc along this certain latitude. Aurora that have this typical shape are thought to have a sheetlike structures with along-arc symmetry [6]. This assumes that the aurora is uniform along a line of constant magnetic latitude [7].

1.1.4 Auroral Arcs

Discrete auroral arcs are caused by electrons exciting molecules in the thermosphere.[3] These excited molecules emit photons which are the visible phenomena we experience when we see the aurora borealis as seen in Figure 1.3. The aurora can be a variety of colors, from pinks and purples to greens and blues. The wavelength of the aurora corresponds to the altitude and kind of molecule that is in the collision which will be either oxygen or nitrogen depending on the altitude. In our study, we will primarily see red aurora, corresponding to atomic oxygen emitting 630.0 nm light, and green aurora, corresponding to atomic oxygen emitting 557.7 nm light [8].

There are two main ways of measuring parameters associated with the aurora: imaging and in situ. Imaging is done with cameras from the ground or from a spacecraft. These cameras record images and are filtered to particular wavelengths of auroral emissions. Although we can collect significant data from imaging, it does not deliver all of the information we need. 3D density profiles can be synthesized from multiwavelength imaging data from multiple locations; however, not everything is visible in the imaging spectrum. Additionally, we can observe the same light signature from different particles, which is ambiguous. To gather the necessary information we need for analysis, we can take measurements of the auroral parameters using sounding rockets and corresponding ejectable subpayloads which fly through the aurora to take in situ or "in place" data. The combination of imaging and in situ data sets create a heterogeneous data set to fully analyze the aurora and corresponding ionospheric structure.

Within these data sets, various types of data are collected to characterize the aurora and corresponding ionospheric structure. Among these parameters are thermal ion temperature, thermal electron temperature, plasma density, and the electric and magnetic field along the trajectory of the rockets. These measurements are made by a family of scientific instruments made by the 317 Rocket Lab and other collaborating labs. The instruments made specifically

[3] The thermosphere is the overlap of the neutral atmosphere and the ionosphere.

by the 317 Rocket Lab will measure thermal ion temperature and plasma density.

1.2 Sounding Rockets

The aurora we are studying necessitates a sounding rocket apogee altitude of about 300 kilometers above the surface of the Earth [6]. This range is above balloon altitude, a typical atmospheric data collection method, but below a sustainable LEO (low Earth orbit) altitude. Sounding rockets are necessary for the mission because they provide a low-altitude, high-cadence platform for ionospheric case study observations [9]. Sounding rockets are small, relatively affordable rockets that are launched into the atmosphere without entering orbit for the purposes of data collection. The rocket trajectories are parabolic and typically last about five to twenty minutes [10].

Sounding rockets are appealing for research because they are relatively inexpensive [9]. They do not require the large rocket boosters or the sustained telemetry that orbiting satellites and rockets require for longer missions. Additionally, the scientific instruments on the rocket, called payloads, are typically recovered post launch, so they can often be reused to decrease recurring costs [9]. Therefore, the same rocket design can be used for multiple launches. Often, the only element that changes between launches is the scientific instruments or the payload. Because of the small amount of change, the mechanical planning for the rocket mission takes less time, allowing for rapid flexibility in experimental planning. In the case of our mission, large parts of the rocket (motors, boosters, skins, etc.) will be recovered, though not reused. Smaller parts of the mission, such as the ejectable subpayloads for example, will not be collected by the team. However, they will have a bounty on them, meaning they can be returned by the public for a reward.

The uses for sounding rockets began with the military and now serve scientific purposes, particularly within solar and geophysical studies [9]. Some use sounding rockets to perform experiments in zero gravity. Others use this altitude to have better visual access for telescopes. In our case, we take advantage of the apogee height to obtain in situ data of auroral behavior in the thermosphere.

We work with the NASA Sounding Rocket Operations Contract (NSROC) to integrate our scientific instrumentation onto the sounding rockets and to launch the rockets at one of their various launch locations. We will launch the rockets from Poker Flat Research Range in central Alaska. NSROC has a variety of sounding rockets at their disposal. We will be using a Terrier-Black Brant sounding rocket. This was determined by the required apogee of the given mission [10].

1.3 GNEISS Mission

The 317 Rocket Lab has been working on the GNEISS (Geophysical Non-Equilibrium Ionospheric System Science) Rocket mission from Fall 2023, working toward the launch in early 2026. This mission's primary objective is to observe non-idealized, non-sheetlike nightside discrete auroral structures and corresponding ionospheric structure [6]. Most aurora are assumed to have along-arc symmetry, which would look like a thick, straight line of glowing light. However, not all aurora fall into this category. We are looking to study aurora that are the consequence of unstable drivers in the ionosphere, such as unusual solar wind or potential drop behavior. The shape of the aurora is a rigorous diagnostic of the parameters of these local drivers. Studying the instability of these drivers will give us more information about the characteristics of near-Earth space. The ideal candidate for this study is a "pre-midnight, discrete, intense-current, auroral structure with distinct zeroth-order along-arc variation" [6]. This translates to a strong, simple aurora that occurs just before midnight, when the Sun is opposite the launch location.

By observing this type of aurora, we aim to learn more about the combinations of flow, current, and conductivity that actually occur in a driven auroral system [6]. We will be collecting data from a heterogeneous multipoint observational platform that will be interpreted by the GEMINI ionospheric model and then compared with existing auroral models [6].

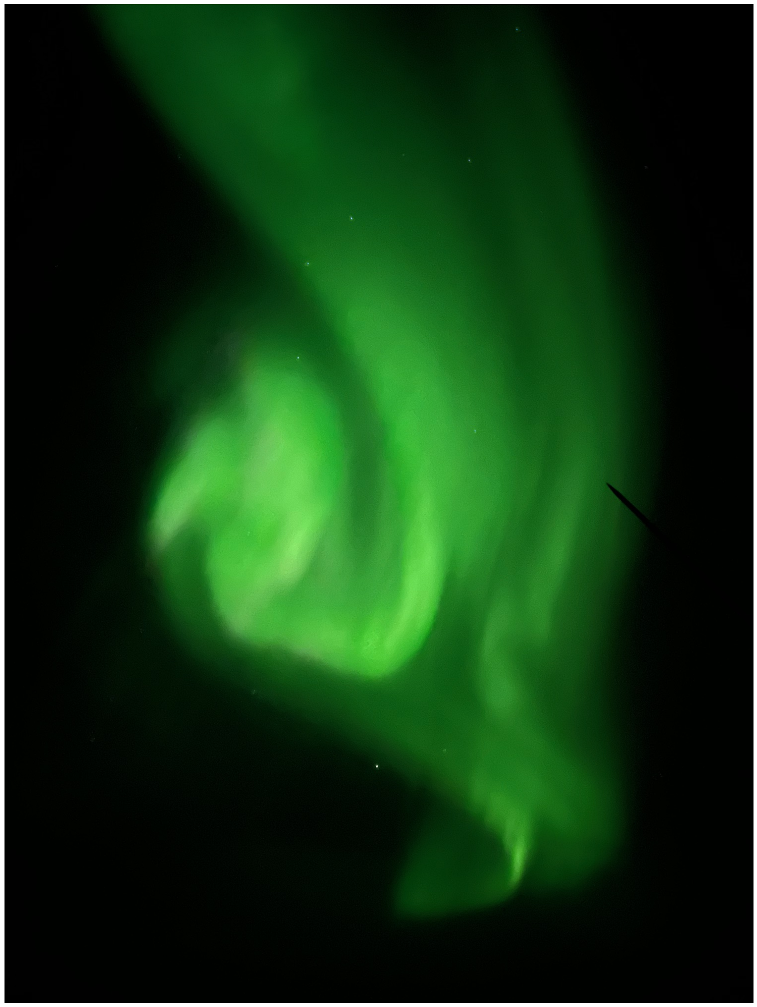

Figure 1.4: Aurora borealis with folds and bends. These features are a consequence of unstable drivers in the magnetosphere. Photo courtesy of Alexander Mule.

As previously mentioned, most aurora are assumed to have along-arc symmetry, but in the GNEISS mission, our goal is to study along-arc variations in aurora. Variations in the lengthwise structures of the aurora, such as folds, bends, and filaments, are typically in the 1-50 km spatial scale, as seen in Figure 1.4 [6]. These variations indicate changes in the ionosphere and its coupling to the magnetosphere. Information about these drivers will reveal information about near-Earth space.

The GNEISS mission will explore along-arc variations in auroral structures by sending two identical sounding rockets through the same auroral structure, but at different locations.

Their proposed trajectories are described in Figure 1.5. Subpayloads will be ejected from each rocket, including two of our Bobs, to gather additional in situ data just off the main payload trajectories. With two rockets, we will be able to see spatial differences between two different slices along the auroral structure. This is the first sounding rocket mission in which the rockets are launched within two minutes of each other which are also azimuthally separated.

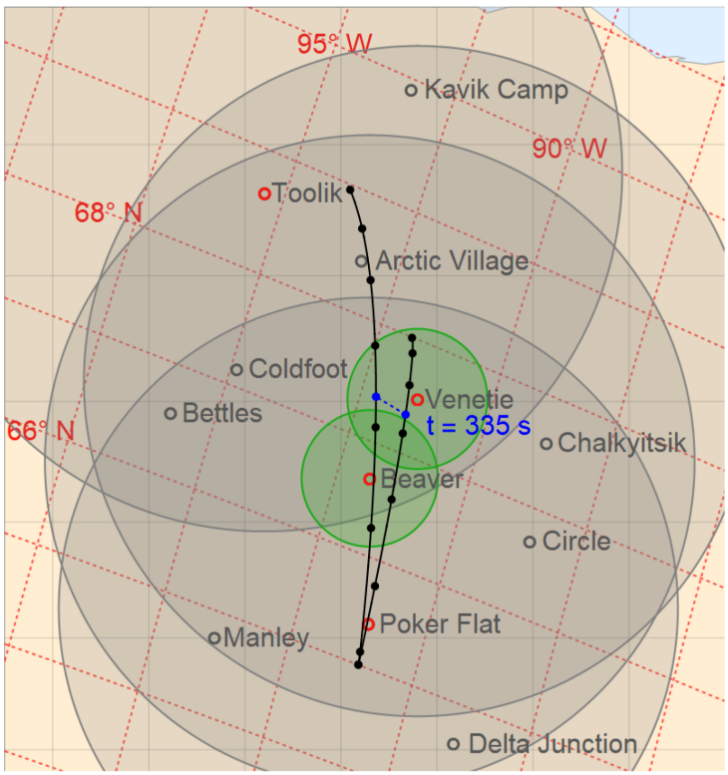

Figure 1.5: Proposed trajectory of the two rockets for the GNEISS mission in rural Alaska. The north-bound trajectories of the sounding rockets are shown in black. The width of the map is equivalent to approximately 600 km. Courtesy of Jules Van Irsel.

The rocket launches will occur during a prespecified flight window in early 2026. Geomagnetic activity will be monitored; when the ideal conditions for the desired auroral structure occur, Prof. Kristina Lynch will give the signal to launch. We will launch the twin sounding rockets from the Poker Flat Research Range (PFRR) in central Alaska which is run by the Geophysical Institute at the University of Alaska, Fairbanks.

1.4 Data Collected

There are three main types of data collection in this mission [6]. Imaging is done by GBOs (ground-based observatories) stationed throughout rural Alaska. There are also in situ measurements made with the payload instrumentation located on the main payload and the ejectable subpayloads. In addition, Lattice tomography instruments will be used to measure the plasma density below the rockets by sending radio frequency (RF) signals from the main payloads to low-cost antennas throughout rural Alaska. In this thesis, I have both improved and designed hardware for in situ measurements and Lattice beacons. This includes Petite Ion Probes (PIPs) which are located both on the main payload and on the ejected subpayloads, called Bobs. The PIPs are small collimated retarding potential analyzers (RPAs), which will be discussed in detail. The data from the PIPs reveal information about the thermal ion temperature, ion density, and ion drift [11]. The ion density and ion drift contribute to our knowledge of the plasma density.

1.4.1 PIP Data

Our study aims to characterize the ionosphere during the aurora. We assume that the ionosphere is made of singly ionized oxygen which corresponds with the altitude of the rocket trajectories [12]. The ionized gas will have some thermal ion temperature, ion density, and ion drift (also known as bulk velocity), each of which can be extracted from the Gaussian distribution curve of the gas [12].

These three variables, which are interdependent and require multi-parameter fitting, are measured with the PIPs. Each PIP has a set of screens that work together to produce a relative voltage which is rapidly swept between 0 V and 5 V [11]. The ion flux flows through the screens to the PIP anode, forming a current that is recorded during the voltage sweep. The derivative of this graph is used to obtain a differential number flux versus voltage plot which is approximated as a Gaussian distribution (see Figure 1.6). The area under this

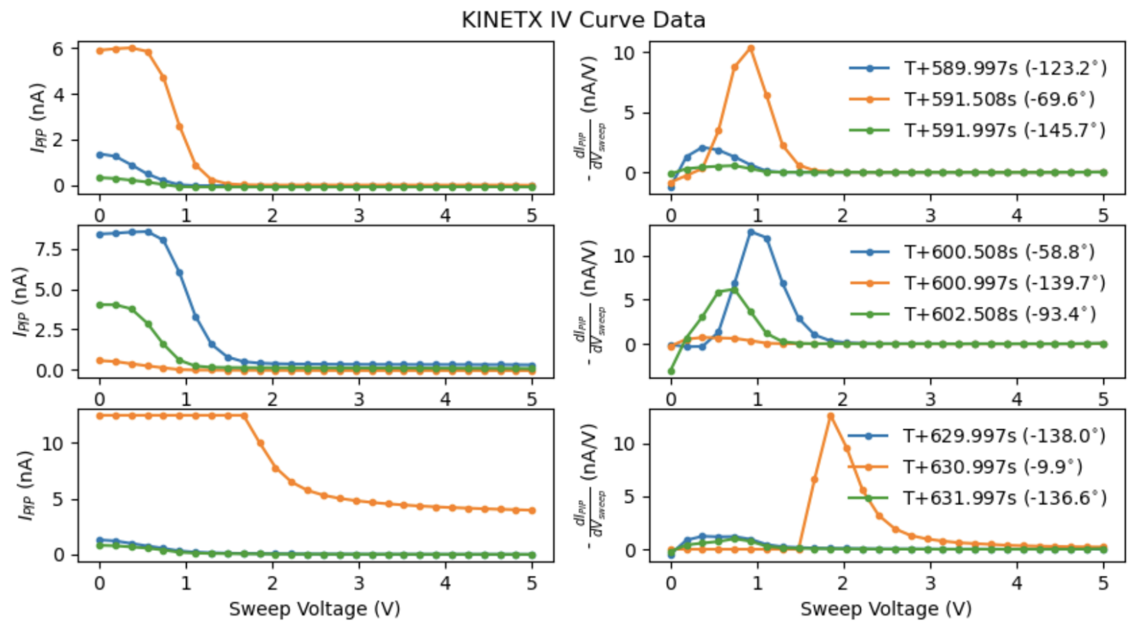

Figure 1.6: Received ionospheric anode current versus sweep screen voltage and differential number flux versus sweep screen voltage at various times during the Kinet-X sounding rocket flight. For a given PIP, the current versus sweep voltage is time dependent because the PIPs move through space and experience different ions flux over time. These data were taken during the Kinet-X experiment. Similar methods will be used for the GNEISS data analysis. Courtesy of Magdalina Moses.

curve corresponds to the ion density, the velocity of the peak signal corresponds to the ion drift, and the half-maximum width corresponds to the thermal ion temperature. These data points are recorded every 22.2 ms [11]. PIPs are positioned at various elevation angles on both the main payload and ejectable subpayloads to obtain measurements of the ion flux along the main trajectories of the rockets and in areas just off the trajectories.

Examples of the collected data are shown in Figure 1.6 which use the Levenberg-Marquardt nonlinear least squares minimization algorithm to analyze the data inferred ionospheric parameter data [11].

1.4.2 Lattice Tomography Data

Lattice tomography is used to gather information about the volume of the thermosphere below the rocket trajectories described in Figure 1.5 [6]. Typically, these parameters are measured from the ground with skyward facing cameras or radars, or with tomography using GPS spacecraft. However, those methods of imaging include information about the volume above the rocket trajectory and do not perfectly distinguish all particle signatures. This new Lattice tomography method only measures the Faraday rotation along lines from the rocket to Lattice receivers[4] located throughout rural Alaska (Figure 1.7). The receivers have two perpendicular RF antennas which work together to determine the polarization of the received signal. There will be one beacon mounted on each of the main GNEISS payloads. The beacon sends out an RF signal which is polarized and will rotate depending on the net plasma density between the transmitter and the receiver, as in a medical MRI scan. A collection of Lattice receivers scattered under the trajectories of the rockets measure the polarization of the RF signal after Faraday rotation.

These data are synthesized similarly to data from an MRI. A set of linear density data is collected, and, with the power of linear algebra, the plasma density of the volume can be determined. Therefore, the beacons and receivers work together to determine the plasma density volume within the volume under the rocket trajectories.

In order to collect the necessary data, instrumentation must be designed and improved upon from previous flights. This includes our most recent mission, Isinglass, which used a previous version of our PIPs and Bobs [11]. The PIP trees, shield board boxes, and Lattice instrumentation, however, are new for the GNEISS mission.

1.5 My Role: Hardware Design

My main goal for this thesis was to improve upon flight hardware in the instrumentation package, or payload, which goes on each of the rockets. Previous missions completed by the 317 Rocket Lab, including Isinglass, used a family of flight hardware that was successful in terms of data acquisition but highlighted areas for improvement in terms of manufacturing

[4] I contributed to the first stages of the Lattice receivers' mechanical design. I decided to make them from low-cost, readily available PVC piping. This material is compatible with rural Alaska's cold and wet weather conditions. Additionally, it can be easily disassembled, shipped to Alaska, and reassembled in the field.

Figure 1.7: Lattice receiver antenna in the field. Courtesy of Alexander Mule

and fabrication side [11]. One of my specific goals was making mechanical improvements to the manufacturing and fabrication processes, especially for the PIPs and corresponding Bobs which will be discussed in depth later. Nearly all of the scientific instrumentation was manufactured in house at Dartmouth College. Due to the high number of PIPs and other hardware that needed to be made, improvements to the design to simplify the production greatly improved the overall process for the GNEISS mission and benefit and informed all following missions. Additionally, I have designed housing for electronics and various instrumentation support structures. All hardware was designed using SolidWorks 2024.

I have developed all corresponding fabrication processes and timelines for the science team instrumentation as the primary project manager. Aside from designing the hardware, I was in charge of communicating with machinists, staff scientists, and new undergraduate research assistants to move forward with the scientific instrumentation manufacturing process while collaborating with engineers at NSROC to confirm that our instrumentation fit within the parameters necessary for sounding rocket integration.

I will begin by briefly describing the manufacturing principles that guided my design process. These include ways to maximize manufacturing efficiency considering mechanical constraints imposed by the sounding rocket vehicle and industry-standard design practices. Then, I will use this foundation to justify my mechanical design choices for each piece of hardware. I begin with the PIP redesign, starting with their screens. I then describe the Bobs design, including the mass distribution constraints. I will then cover the supporting hardware including the PIP trees, shield board boxes, and Lattice boxes. Each of these is shown in Figure 1.8.

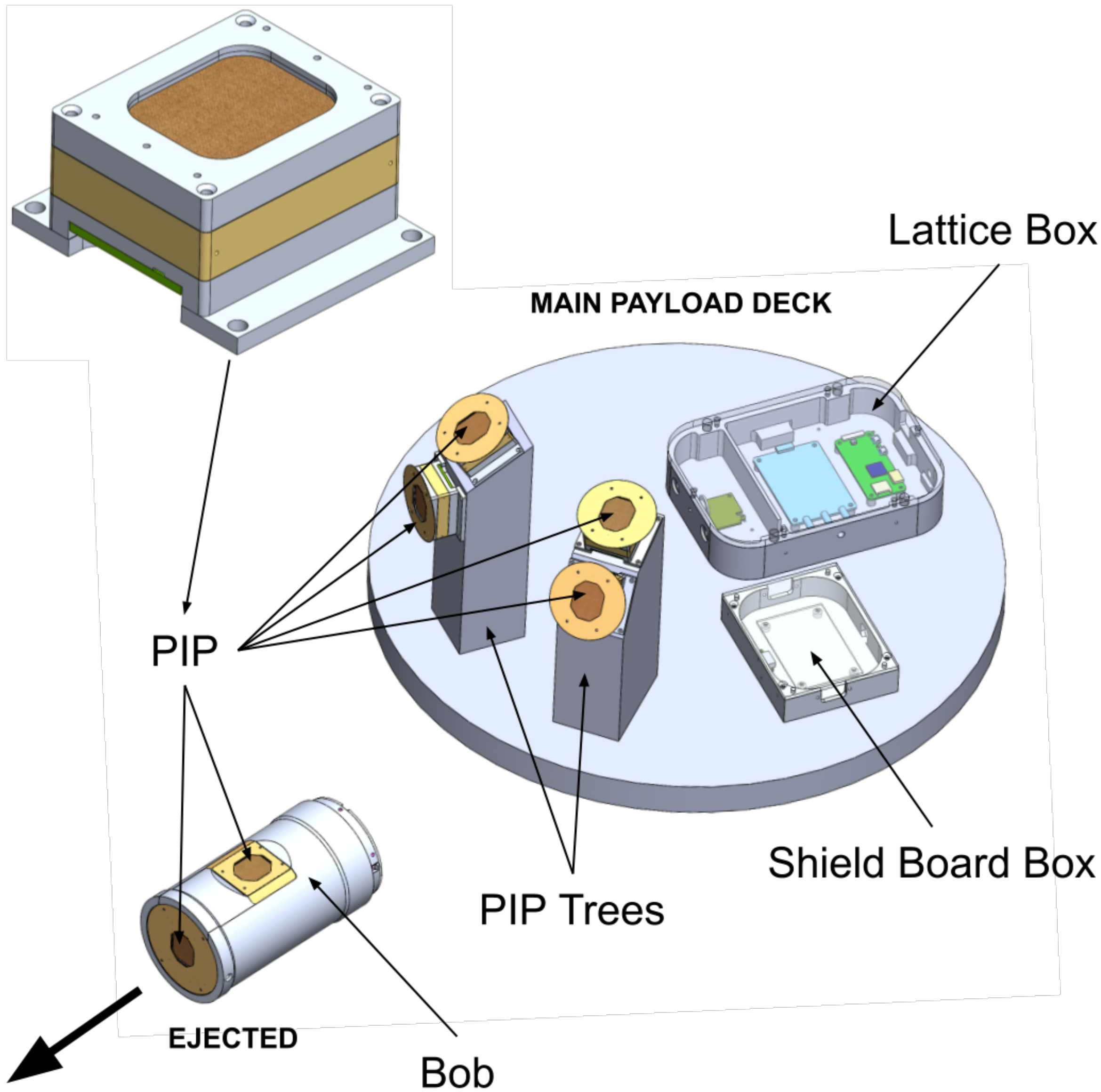

Figure 1.8: GNEISS hardware overview on a mock deck to provide context for the mission hardware. Two PIP trees with PIPs, a shield board box, and a Lattice box are located on the sounding rocket deck. A Bob, which includes two PIPs is ejected from the sounding rocket. The PIPs are outfitted with their location-specific gold planes.

Chapter 2

Design Principles for Sounding Rocket Hardware

For my thesis, I have updated and designed a family of flight hardware to house and mechanically support electrical instrumentation to study aurora. In practice, this means designing parts that geometrically allow the electrical hardware in our instruments to be configured and mounted while avoiding unwanted electrical connections. When designing hardware for ionospheric flight, sounding rocket constraints, environmental factors, instrumentation, and manufacturing must be kept in mind.

These principles have been applied to the following flight hardware. PIPs are small voltage sweeping devices that measure ionospheric parameters [11]. They are located on both the main sounding rocket payload and on the ejectable subpayloads called Bobs. On the main payload, PIPs are mounted on PIP trees at a variety of elevation angles on each of the main payload decks. There are two decks on the main payload — one on the forward end and one on the aft end. Instrumentation can be mounted onto these internal platforms.

The ejectable Bobs contain two PIPs, a shield board[1], and an IMU (inertial measurement unit[2]). There are also shield boards on the main payload located in shield board boxes. In

[1]The shield board, a printed circuit board, was designed by undergraduate students and a staff engineer in the 317 Rocket Lab. It electrically controls and queries the PIPs.

[2]IMUs are commercially available PCBs which measure acceleration, magnetic field, and angular velocity

addition to the shield board boxes, there are also Lattice boxes which emit RF signals through the atmosphere to multiple Lattice receivers located throughout rural Alaska. Each of these elements are designed with the design principles described in the following sections.

2.1 Sounding Rocket Constraints

2.1.1 Mass

Sounding rocket flight trajectory parameters, such as the apogee altitude, are directly determined by the type of sounding rocket and total mass [13]. For our study, the trajectories of the sounding rockets are chosen by the predicted location of the aurora. Ideally, we would determine the total mass of the payload early in the design process so that the correct rocket and launch angle can be determined to obtain the preferable flight path. It is better to err on the side of less mass because it is much logistically easier to add mass than to eliminate mass from essential instrumentation. During rocket design, there are plenty of parameters at play, so flexibility is key.

Metals, such as aluminum, are used because they are lightweight, low-cost materials. Additionally, mass is removed from hardware wherever necessary. Significant thought goes into these mass-removal design decisions. Mass distribution is especially important to consider to manage coning of the main payloads and the Bobs, seen in Figure 2.1, during flight.

Coning happens when the angular momentum and angular velocity vectors are not parallel. The Bob's internal components were intentionally placed to diagonalize the inertia tensor while constraining one of the principal axes to the intended primary rotational symmetry axis of the subpayload. This was a particular challenge because the internal components of the Bobs are not symmetrical, primarily because of the side PIP which faces radially outward. Custom longerons and electrical housing were created to balance the side PIP's mass contribution which ultimately diagonalized the inertia tensor. This design challenge will be

along three perpendicular axes.

discussed further in the Bob chapter.

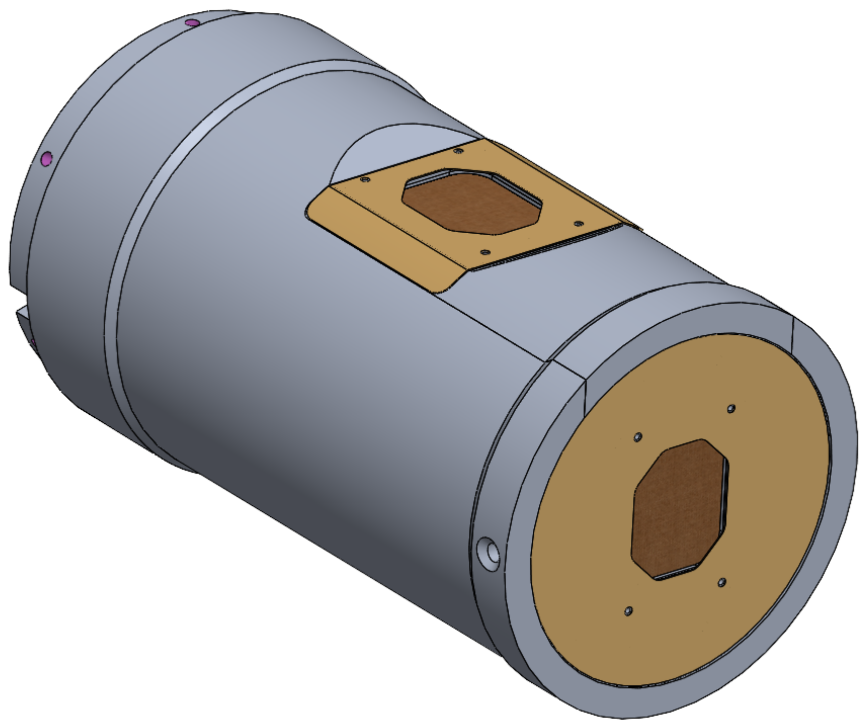

Figure 2.1: The Bob, an ejectable subpayload, was designed with an intentional mass distribution to prevent coning. The total length is 6.225 inches.

2.1.2 Spacing and Sizing

Each of the hardware components on the payload decks must also be thoughtfully placed to diagonalize the inertia tensor and to prevent excessive coning in the main payload.

Flight hardware is spatially minimized to fit inside the minimal deck space available for instrumentation. On the GNEISS rocket, there are several instrumentation packages that need their own space on the decks. Aside from the physical boxes and instruments, space must also be reserved for wired connections between components. Although they may seem negligible, connectors can often take up much more room than expected, especially in the regions where they connect to instruments.

When deciding on the layout for a payload deck, accessibility must be considered. Components of the payload may need to be reached during preflight checks through payload skin doors [13]. Limited volume and accessibility became important factors when designing the Lattice boxes as seen in Figure 2.2. We had the opportunity to include our Lattice boxes on another flight to test our Lattice tomography experiment. Because the flight decks already had several other instrumentation packages, I had to work diligently to fit our box onto a deck. In fact, the outer corners have large radii to fit within a tight space between another box and the skin of the sounding rocket. Additionally, the external connector ports were intentionally placed to be reachable from a nearby access door.

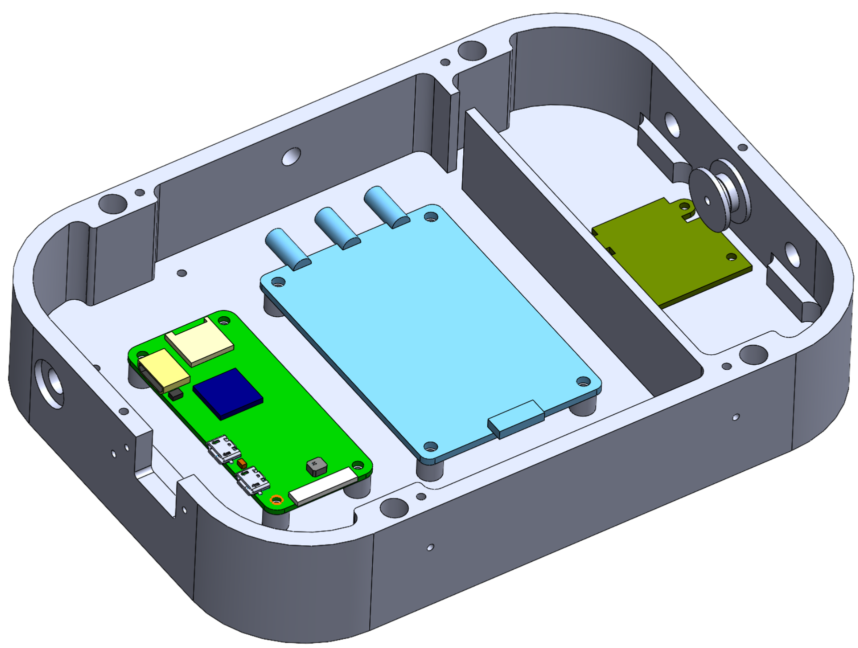

Figure 2.2: Lattice box spacing and sizing. The internal volume is large enough to house all of the necessary electronics while minimizing its size to fit onto a spatially constrained sounding rocket deck. The Lattice box is 6” in length.

2.2 Environmental Constraints

2.2.1 Venting

Over the sounding rockets' trajectories, they will quickly reach altitudes with little to no atmospheric pressure. In these vacuum-like environments, pockets of air, under a screw for example, will not immediately equalize in pressure. This could result in a slow gas leak from the trapped volume. These molecules in the leak could tamper with the ionospheric instrument measurements which are sensitive to low pressures in the atmosphere. Vents are used to allow gasses to escape quickly during launch, ensuring that slow gas leaks do not occur later during data collection. For example, vents were used in the PIP brass piece, as seen in Figure 2.3, to prevent slow gas leaks from the tapped holes.

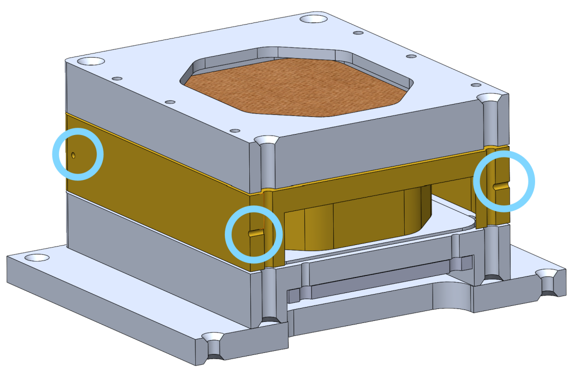

Figure 2.3: PIP brass spacing piece vents are circled in blue. This is a section view of the PIP. The PIP is 1.7" in length.

2.2.2 Vibration

During launch, the sounding rocket and internal components are subjected to substantial vibration. With enough vibration, components can become dislodged from their functional position. For example, screws can be vibrated out of their tapped hole if not designed correctly. This could allow components to become dismounted and nonfunctional, possibly leading to a data acquisition failure. Special screws can be used, such as one with thread-locking, to prevent dislodgement. Vibration can also be minimized by avoiding structures with long, thin ends which are subjected to greater deflection. For example, later iterations of the PIP trees eliminated long, thin free ends to prevent excessive displacement with vibration as seen in Figure 2.4. This is because of the second moment of area which will be discussed in the PIP tree section. For cantilever beams with one fixed end and one free end, the deflection at the end is indirectly proportional to the second moment of area [14]. By increasing the second moment of area, we can decrease the observed deflection. All flight hardware will undergo vibration testing prior to flight.

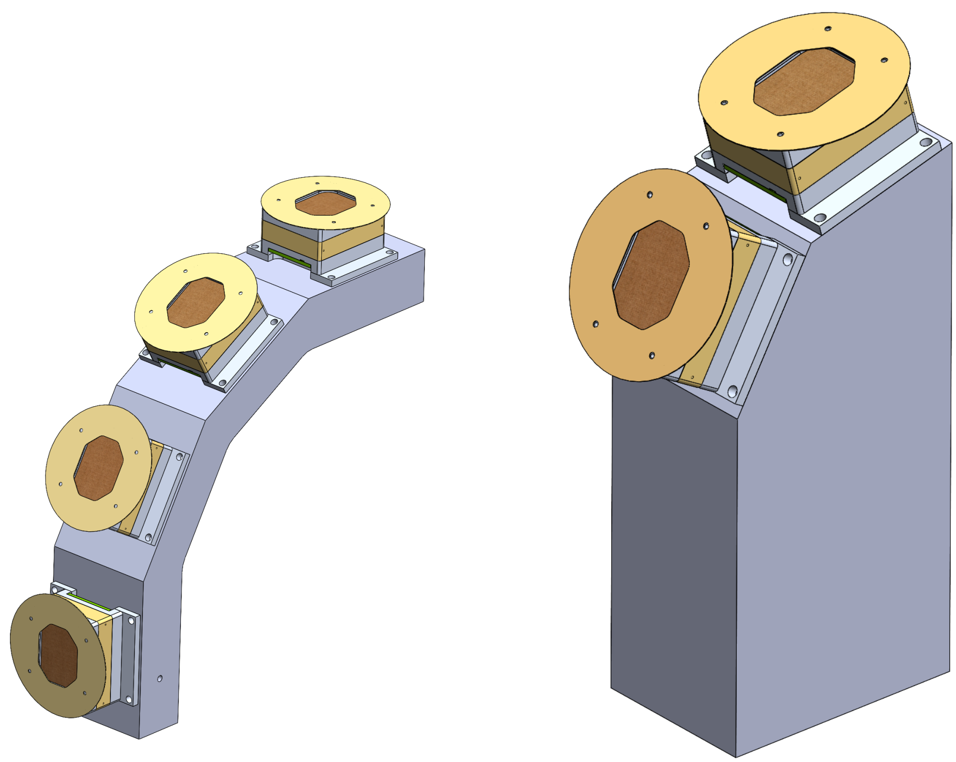

Figure 2.4: PIP tree improvements included eliminated long, thin free ends to minimize effects of vibration. The PIP tree on the left is a previous iteration while the PIP tree on the right displays these changes. In addition, the PIPs were separated onto two different PIP trees on each deck to have PIPs at different deck clock angles. Although the different PIP trees vary, they are approximately 6" tall.

2.2.3 Temperature

During the trajectory, the sounding rocket travels through many different altitudes. Typically, heat generated by electrical components is the primary thermal considerations, since, in a vacuum, there are only radiative and conductive cooling but no convective cooling from air. For example, the aluminum floor served as a heat sink for the power amplifier in the Lattice box because it produces significant heat. On the other hand, our Lattice receivers are distributed throughout rural Alaska and had to be made out of materials that can function at temperatures well below freezing. We had to consider compatible epoxies, zip-ties, and power cables.

Because the flight hardware is only exposed to the elements for a few minutes, we do not have to pay as much attention to factors such as corrosion from oxygen, which can be significant for orbiting spacecraft; or to radiation hardening, another satellite concern.

2.3 Instrumentation Constraints

Throughout our instrumentation, a lot of hardware is made to house PCBs (printed circuit boards) and related electrical components. It is important that these components remain electrically isolated. The conductive areas of the PCBs and connectors must not make electrical contact with the aluminum housing. In order to avoid this, PCBs are elevated on bosses, shown in Figure 2.5, to create a gap between the conductive soldered bumps below the board and the aluminum housing. Bosses are small stubs that align with the mounting holes for the PCBs. The diameter of the bosses is smaller than the non-conductive patch that surrounds each of the mounting holes of the PCBs. Based on the accessibility of the area, bosses can often be machined into the hardware. In some cases, non-conductive bosses can be fastened into tapped holes in the machined housing.

Occasionally, recesses in the housing are created to allow non-conductive portions of the PCBs to make direct contact with the housing while electrically isolating the conductive

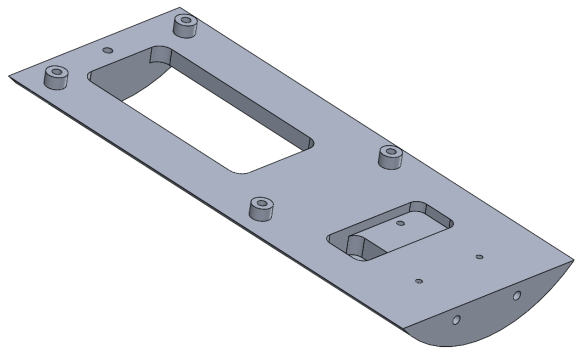

Figure 2.5: Bob cap longeron includes bosses to electrically isolate the shield board. It is 5" in length.

areas. This was a key strategy for setting the IMUs in place on the Bob cap longerons while making space for electrical connections which emerge from the bottom side of the board, as shown in Figure 2.6.

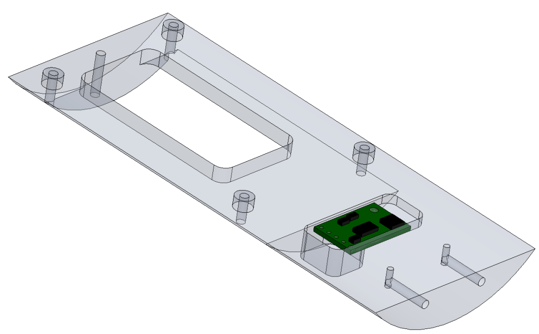

Figure 2.6: Bob extended cap longeron includes a recessed pocket to create room for wires soldered to the bottom side of the IMU. The cap longeron is made transparent in this image to show the recessed pocket. The longeron is 5" in length.

2.4 Manufacturing Limitations

Another essential design principle is to consider manufacturing limitations. Many of the design choices were made as a result of subtractive manufacturing. Subtractive manufacturing is a process where every feature of a part must be made by cutting away material. The geometry of our parts calls for mills. All of our machined pieces are made in house by the Dartmouth Science Division's machine shop. Therefore, our designs are limited by the available manufacturing equipment and corresponding resources.

2.4.1 Cost

Cost must also be considered because we are producing hardware in large quantities. For the early 2026 launch, we will have manufactured thirty-two PIPs, ten main payload shield boxes, eight PIP trees, six Bobs, and four Lattice boxes. Although cost is not the primary limiting factor, it is important to save money where possible. We accomplish this by using low-cost materials and stressing ease of assembly in the design to minimize labor. This is done by making easily manufacturable designs. For example, for easily programmable cuts on the mill, I try to make the dimensions of my designs clean numbers that make the machinists' jobs as straightforward as possible. Additionally, I made the majority of the features in the parts in ways that minimize the number of tool changes and part set-ups.

2.4.2 Symmetry

Another unexpected tool for manufacturing ease, especially when it comes to fabrication, is symmetry in parts. Not only does this make each part more simple to machine, but symmetrical parts are also easier to install during fabrication. There are simply fewer ways for a person to err. This is key for a project on this scale. In some cases, exaggerated asymmetry can also prevent errors. The danger lies within slight asymmetries.

2.4.3 Mills and Machining

The majority of the parts are made on a 2.5 axis mill. These mills have freedom to move along three orthogonal axes. However, tool passes can only be made at a constant height at a time. Most of the machining will use CNC which codes a path for the mill. However, the path still has to be coded by the machinist. Mills work by rapidly spinning an end mill which can be lowered to a certain height along the z-axis to make a cut. The part is held tightly in a vise and moved slowly along the x- and y-axes to shave off material along a determined path.

During the cut, the side of the end-mill takes material off the side of the part. As the end mill gets smaller in diameter and the depth of the cut increases, the deflection and chatter of the end mill will increase. Too much deflection will result in off-nominal parts and subpar surface finishes. I designed each part with this in mind. For example, this limits the maximum pocket depth for parts made with the end mill. A pocket is a machining operation which features a flat cut with a closed boundary, like an empty swimming pool in the ground. As pockets are cut, a larger end mill is used to start to take out material efficiently. This would leave large rounded corners in a rectangular pocket. Typically, a smaller end mill would then have to be put into the mill to cut corners with smaller radii. Whenever possible, I used large fillets (rounded corners) in pocket corners to minimize the number of times a new end mill would need to be put into the mill to cut smaller and smaller radii. By using these larger fillet edges, thicker end mills could be used which is helpful when significant depth is necessary. This was the case for the shield board box pocket as shown in Figure 2.7.

2.4.4 Wall Thickness

There are also general design principles that specifically guided the design of machined parts. In order to maintain machinable designs, I had to pay attention to the limiting widths of machined sections. Especially on small parts within the PIPs, wall thickness can be very small. It is important to maintain a certain wall thickness to prevent distortion. This is particularly important when there are tapped holes close to the edge of a part. Tapped holes are threaded to engage with a specific type of screw. To create them, a uniform hole is

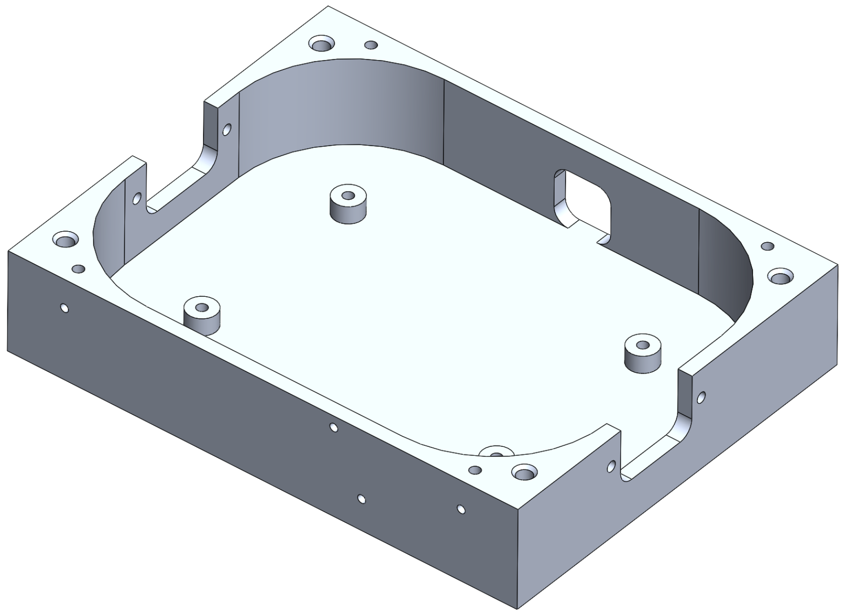

Figure 2.7: The pocket of the main payload shield board box has large fillets to minimize the number of tool changes. The box is 4.5” in length.

drilled to the minor diameter of the thread. Then, a tool called a tap is used to carve away material to make the threads. Even if the hole may seem far from the edge, it is possible for the tapping process to push material outward, making the outer surface off-nominal. Thicker wall thicknesses can prevent this from happening.

The issue of thin walls surfaced when designing the top housing for the PIPs. At first, I placed the tapped holes for the gold planes along the long edge of the housing. In a previous design iteration, there was plenty of room between the pocket for the screens and the edge of the part. However, along the design process, I expanded the screen pocket to make room for electrically isolating tape and extra tolerance. This made the wall thickness between the tapped hole and the edge of the part too small. I decided to move the holes to the short edge of the top housing which could provide substantial wall thickness, as shown in Figure 2.8.

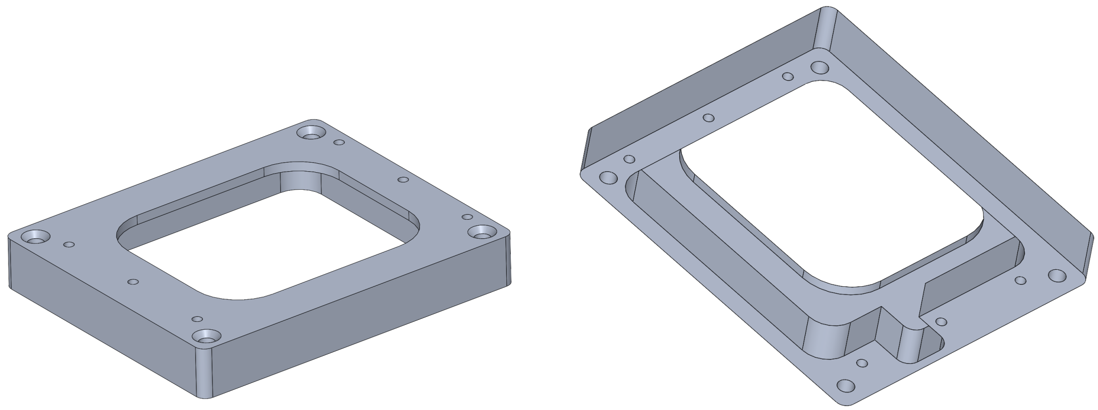

Figure 2.8: PIP top housing piece has thin but sufficient wall thicknesses to minimize volume and mass while still maintaining enough material to keep the design machinable. The piece is 1.7" in length.

2.4.5 Machining Access

Cutting access must also be considered. Some cuts on the 2.5 axis mill are impossible to make. If parts are cut with an end mill, everything above the cut feature must also be cut or not exist in the first place (see Figure 2.9). In these cases, parts can be made separately and assembled later. This was done for the Bob cap, as shown in Figure 2.10. To make assembly more efficient, I expanded the role of the cap to also house all of the internal Bob instrumentation. This means including an additional longeron feature on the cap. If the part were kept whole, the bosses on the cap longeron would have been inaccessible for the mill because of the cap L-bracket above. The part was made into three pieces (the cap disc, the cap L-bracket, and the cap longeron) to make each feature machinable.

2.5 Design Principles Conclusions

Now that the basic principles and processes of my designs have been laid out, I will now walk through each of the flight hardware elements I made for my thesis and the corresponding reasoning behind their designs. This flight hardware package includes PIPs, Bobs, PIP trees, shield board boxes, and Lattice boxes. I have carefully integrated the principles described

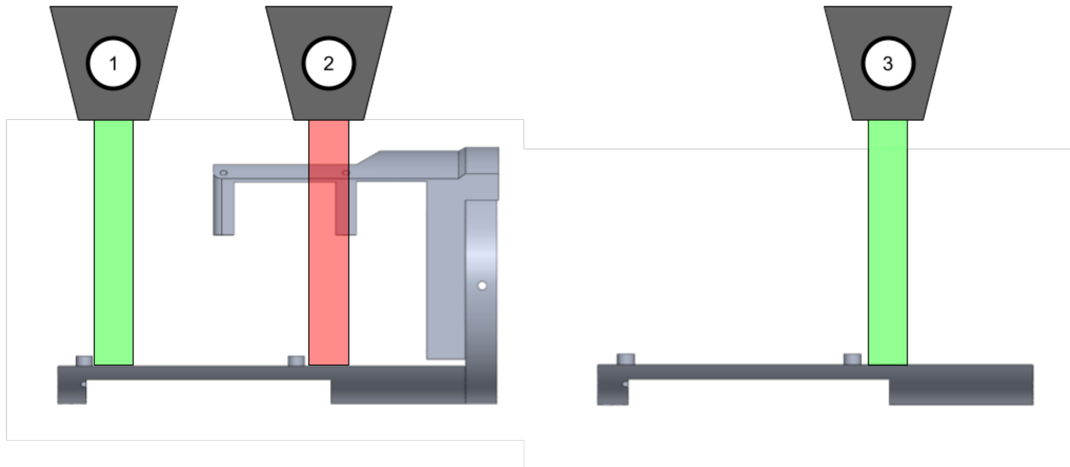

Figure 2.9: End mill machining access. In end mill configuration 1, the end mill has complete cutting access to the Bob cap longeron on the left side. However, it will not have cutting access in end mill configuration 2 because the Bob cap L-bracket is in the way. If the Bob cap is separated into multiple sections, we can achieve complete cutting exhibited in end mill configuration 3.

above to produce new parts and to improve previous flight hardware.

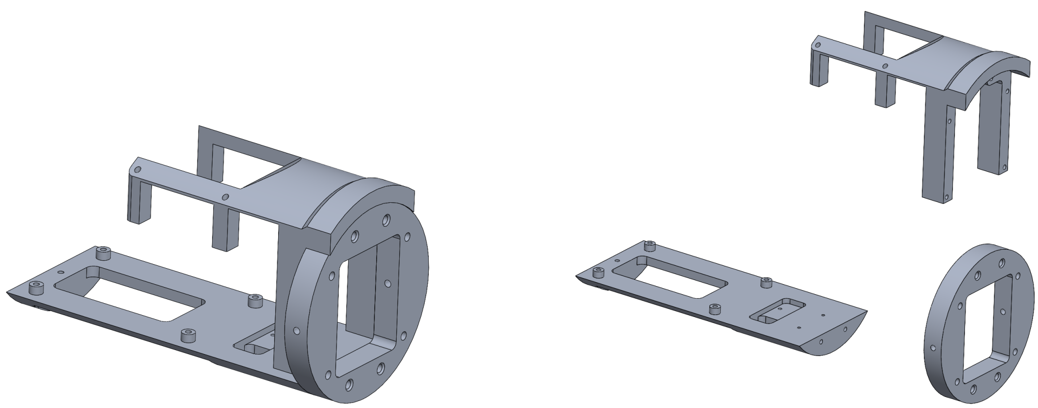

Figure 2.10: The Bob's extended cap had to be separated into three pieces (the cap disc, the cap L-bracket, and the cap longeron) because of limited machining access. The Bob cap is 5.41” in length.

Chapter 3

Petite Ion Probes

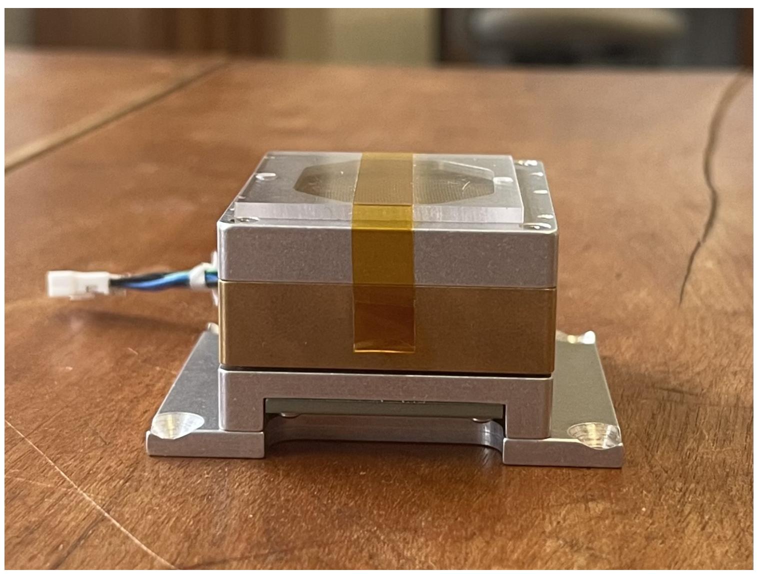

Figure 3.1: Fully fabricated PIP with protective plastic cover. Photo courtesy of Sean Wallace.

Petite Ion Probes (PIPs), shown in Figure 3.1, are responsible for measuring the ionospheric response to the existence of the aurora. The influx of electrons due to the magnetosphere's snap causes ambient activity in the ionosphere. Studying this activity is one of the main goals of the GNEISS mission. The PIPs do this by collecting in situ data such as thermal ion temperature, ion density, and ion drift. Each of these variables contributes to the heterogeneous multipoint dataset that the GNEISS mission will collect. There are PIPs located on each of the ejectable subpayloads and on the main payloads, so data can be taken along the trajectory of the main payloads and in nearby areas.

For the GNEISS mission, we will need to build twenty-four flight PIPs along with extras for bench tests and spares (see Appendix A). In previous flight missions, there have been a few key manufacturing inefficiencies that have made the high-volume production process more difficult than necessary. I have made improvements to the mechanical design of the PIPs while maintaining their electrical functionality to expedite the manufacturing process.

3.1 Screens

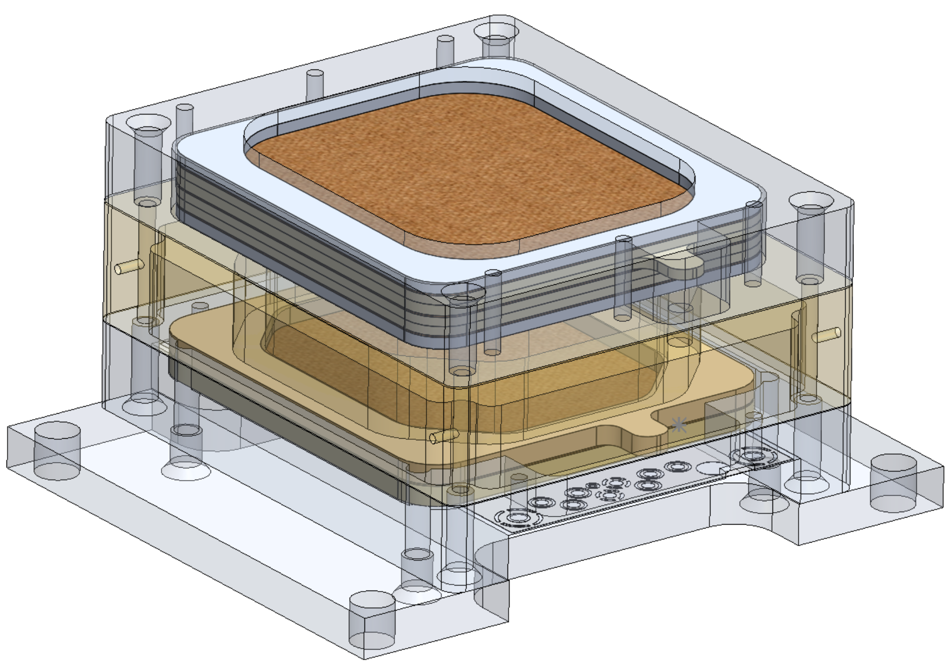

Figure 3.2: PIP model highlighting screen placement. The top housing, brass piece, bottom housing, preamp board, and base plate appear transparent in this image to clarify the screen placement. On top, the top ground screen, sweep screen, and bottom ground screen are stacked and clamped to the brass piece with the top housing. On the bottom, the suppression screen is clamped up to the brass piece with the bottom housing. The outer dimensions at the base of the PIP are 2" by 1.7". The PIP is 0.987" tall without the gold plane.

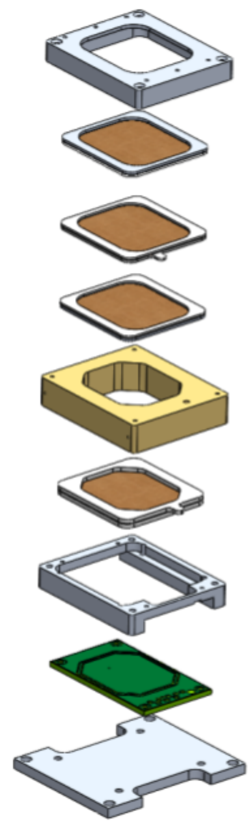

Figure 3.3: PIP expanded view. From top to bottom, there is the top housing, top ground screen, sweep screen, bottom ground screen, brass piece, suppression screen, bottom housing, preamp board with an anode, then the base plate.

3.1.1 Screen Overview

In terms of electrical elements, each PIP contains four different screens with conductive mesh and an anode on the preamp board as shown in Figure 3.2. Following the path that an ion would take through the PIP (top to bottom), there is a top ground screen, a sweep screen, a bottom ground screen, a brass piece for separation, a suppression screen, then an anode. The ground screens and sweep screen together make the "top screen stack."[1] The order is

[1]In this chapter, I often refer to the screen stack in terms of what needs to be clamped by either the top or bottom housing. The same mechanics are used to clamp the top screen stack with the top housing and

shown in detail in Figure 3.3. During flight, the sweep screen is programmed to quickly sweep between 0 V and 5 V to regulate the ion flux through the screen. The mesh, which is 90% transparent and contains 70 lines-per-inch, sets an equipotential over its plane. The high-transparency mesh allows 90% of the ion flux (with sufficient energy) to pass through the PIP aperture. The ions that have enough energy to make it through the sweep screen will then travel to the anode which is located on the preamp board. The ions will land on the anode which reads the current as a signal. Along the way, the ions pass through the suppression screen which guides any ions that are struck off the anode back to the anode to ensure that the current that is measured is from the ambient ionosphere. The signal is then processed by the shield board, which converts the current to a voltage and digitizes it, and is later analyzed post-mission. The shield boards are individually calibrated to each pair of PIPs.

Pads in the preamp board are electrically connected to the sweep screen and the suppression screen to set their voltages. These screens each have a tab that is electrically connected to their conductive mesh. Straight metal pins are used to connect each the sweep screen tab and the suppression screen to their corresponding pads on the preamp board.

Each screen has two screen frames. The sweep screen and suppression screens use two PCB[2] frames which isolate their conductive mesh from the surrounding conductive housing. The two ground screens have one PCB screen and one aluminum screen which puts the conductive mesh in electrical contact with the housing, keeping the screen electrically grounded.

One design factor that is important to keep consistent between the old PIP design and the new one is the inner volume of the PIP. The specified area, height, and aperture are used in the analysis to calculate the desired ionospheric parameters. In order to keep the

to clamp the suppression screen with the bottom housing. For the sake of simplicity, I will refer to both the top screen stack and the suppression screen as "screen stack" even though only one screen is in the bottom screen stack.

[2]Because of the electrical needs of the non-grounding screen frames, custom made PCBs with a non-conductive base and specifically placed electrical pads are a straight-forward, purchasable solution.

analysis tool consistent between missions, we will keep the area of the aperture and the height between the top ground screen and the anode the same as before. Although this may seem trivial, other design constraints, which will be discussed later in this chapter, complicate the height of the screen stacks.

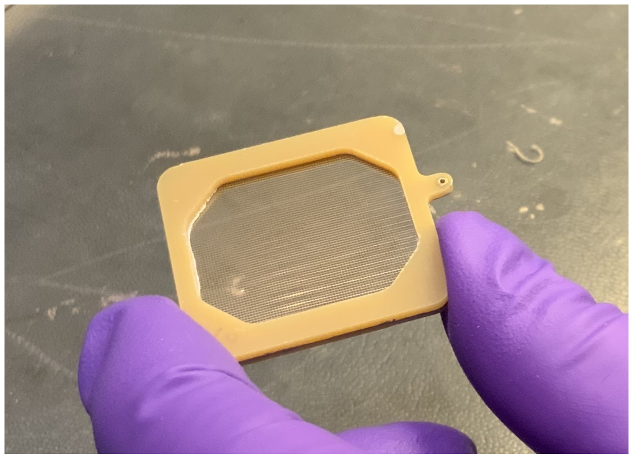

Figure 3.4: Suppression screen during fabrication. Photo courtesy of Rowan Kowalsky.

3.1.2 Screen Improvements

Significant design changes were made to the screen manufacturing process. For context, each screen is made of two screen frames that sandwich the conductive mesh, as shown in Figure 3.4. During fabrication, the conductive mesh must be carefully flattened and secured on top of one frame before the top frame is placed on top with epoxy. I designed a new screen jig, shown in Figure 3.5, to align each of the frames. The conductive mesh is notoriously difficult to work with, so the fabrication of hundreds of screens is tedious and indicates an area for improvement.

In previous fabrication rounds, only one screen was made at a time using the jig to align the top and bottom frames for each screen. I designed[3] the new screen jig to simultaneously fabricate four screens — one of each in a PIP set. The base of the jig features four pockets

[3]The screen jig design was a collaboration between staff scientists Alan Goldblatt and Rowan Kowalsky, machinist Kye Cooley, and myself.

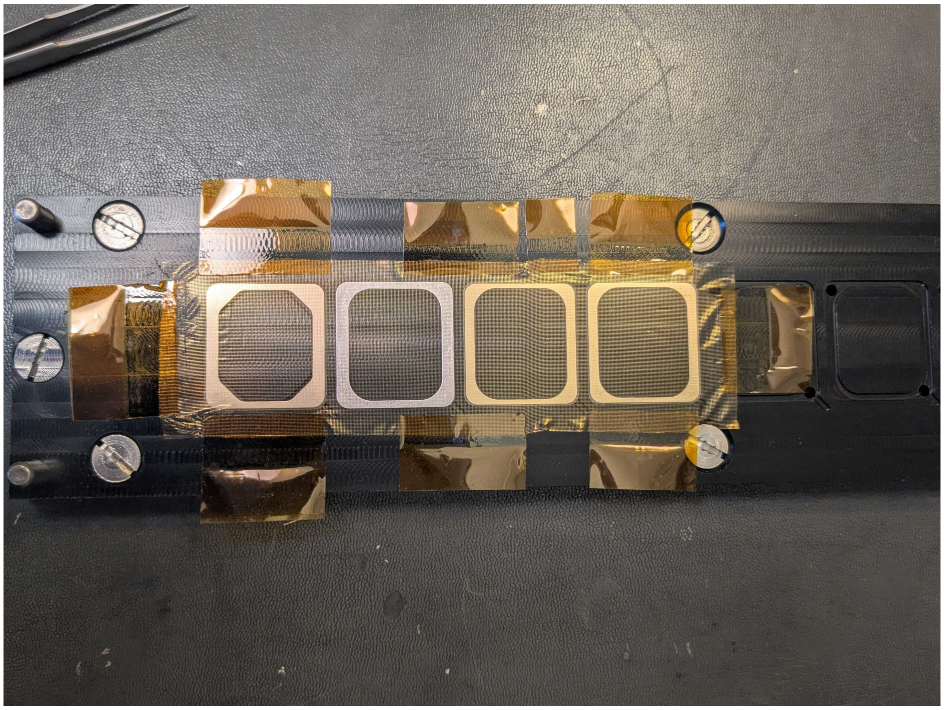

Figure 3.5: One set of PIP screens during fabrication in the new screen jig. From left to right, there is a suppression screen frame, ground screen metal frame, sweep screen PCB frame, and then a ground screen PCB frame, each with no tabs. This layer of screen frames are in pockets, making them flush with the jig surface. A layer of mesh is taped tautly to the jig surface. Photo courtesy of Rowan Kowalsky.

which correspond to the profile and thickness of each unique screen frame. This way, a screen's bottom screen frame could be inserted in the jig to create a flat plane for the conductive mesh. Then, a stencil corresponding to the top screen frames is laid on top, so a layer of epoxy and the top screen frame could be perfectly aligned to the bottom screen frames.

Additionally, in the previous screen design, the corners of the screen frames had clearance holes in them to mount them to the rest of the PIP housing, as shown in Figure 3.6. The conductive mesh sandwiched between the frames had to be completely cleared by tediously poking out of these holes to insert the screws without risking an electrical short. This required in excessive time and labor.

The new PIP design, described in the following sections, features screens with no clearance

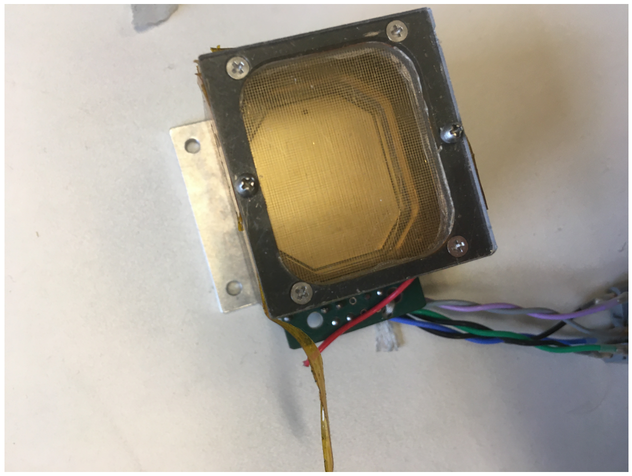

Figure 3.6: Top view of old PIP design with screws threaded through holes in each of the screens. Photo courtesy of Prof. Kristina Lynch.

holes for screws. Instead of clamping the screens down with screws, my new design uses a top housing piece to clamp the top screen stack down onto the brass piece. Similarly, the bottom housing piece is used to clamp the suppression screen up onto the other side of the brass piece. Clamping the screens into place eliminates the extra labor needed to clear the screen holes of any mesh. However, it invites errors in spacing and compression if the parts are not designed correctly with necessary tolerances. The top housing, bottom housing, and brass pieces work together to align and correctly space the screens. The next section will describe the design choices for each of these parts.

3.1.3 Screen Design and Fabrication

Now that the function of the top three screens has been described, I will describe the mechanical structure of the screens. The screens are nominally all 1.200" by 1.300". The metal frames used in the ground screens are nominally 0.030" thick, the sweep and ground PCB screen frames are nominally 0.03125" thick, and the suppression PCB screen frames are nominally 0.0625" thick. However, the PCB screen frames tend to vary by a couple of thousandths of an inch depending on the stock material used. We order the PCB frames from a third party manufacturer, and it is not possible to put strict tolerances on these pieces.

Because of the needed consistency in distance between the top ground screen and the anode, the screen thicknesses needed to have some sort of reliable consistency. We could not ask this of the manufacturer, so I had to adapt my design to the true dimensions. We ordered all of the PCB screen frames we needed and measured all of the thicknesses. I averaged the height for each type of screen and used this value to calculate the pocket depth to house the screens.

Not only were the PCB screen frames various heights, but the epoxy layer used to assemble the mesh and the screen frames contributed an unknown, inconsistent thickness. In order to account for this, multiple sets of fully manufactured screens were made, measured, and averaged to get more accurate top screen stack and suppression screen heights. This was also motivation to make the screen fabrication process uniform and consistent, which was partly improved by the new jig. We erred on the side of a shallow pocket to house the screen stacks because this would still allow for clamping to be effective if a pocket were deeper than the screen stack thickness. Ultimately, we decided to make the pocket depth 0.005" shallower than the nominal expected screen stack thickness to leave excess space to maintain clamping contact if the stack erred on the shorter side. This small gap between the housing and the brass piece also serves as a vent for the screws used to mount the top and bottom housing, as discussed in the design constraints chapter.

As of April 15th, 2025, all of the screen fabrication has been completed. Now, the screen fabrication team is working on assembling the stacks of screens to prepare for PIP fabrication.

3.2 Top Housing Design

The top housing, shown in Figure 3.7, clamps the top screen stack down onto the brass piece. The top housing has several key features. The screen pocket on the underside of the piece is 0.195" deep to house the nominally 0.200" top screen stack. The 0.005" that protrudes out

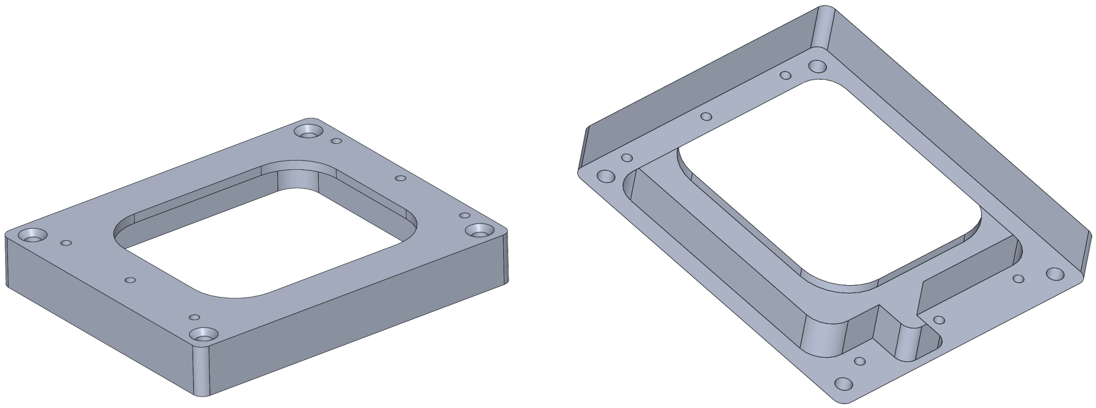

Figure 3.7: PIP top housing piece top view (left) and bottom view (right). The outer dimensions of the housing are 1.4” by 1.7”.

of the pocket allows the screens to be clamped down even if the screen stack is 0.005” under the nominal screen stack height. The averaged screen stack heights presented a ± 0.004” tolerance. As previously mentioned, this small gap will also serve as ventilation for trapped air.

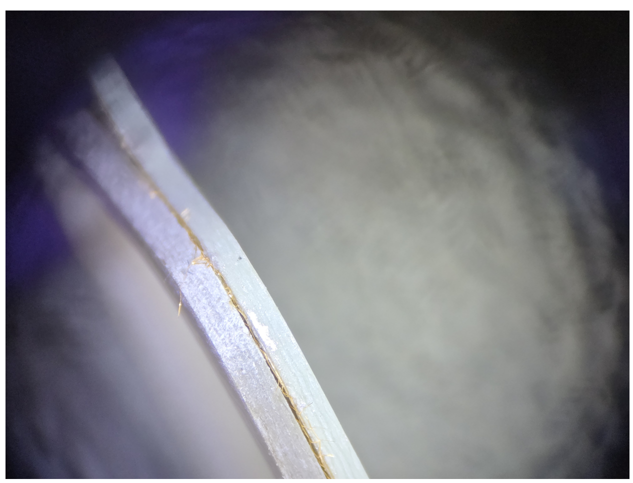

Figure 3.8: Side view of ground screen. Fibers from the conductive mesh protrude from the sides of the screen frames after fabrication. Photo courtesy of Rowan Kowalsky.

The pocket length and width are 1.320” and 1.220”, respectively, to match the screen dimensions with a 0.010” clearance on each side to make room for a layer of 0.005” thick electrically insulating tape with extra room for tolerance. This tape is a necessary addition because some of the screen mesh pokes out from the screen sides, even after a razor blade cleaning, as shown in Figure 3.8. Without tape, this mesh would touch the aluminum top housing, grounding the screens and resulting in an inaccurate voltage value. If this happened to a sweep screen, it would render the PIP useless.

The pocket length and width also had to be sized with screen dimension tolerances in mind. During the screen fabrication process, the top and bottom screen frames in a screen are not always perfectly aligned. There tends to be a slight overbite (0.001" - 0.003") due to the over-sized pocket in the screen jig to accommodate larger-than-nominal screen frames. The slight widening of the top housing pocket allows for the overbite, tape, and smaller-than-nominal manufactured top housing to still fit together.

This allows the screens to shift a maximum of 0.010" inches from their nominal position. This is acceptable because the aperture for the ions to pass through the volume of the PIP to the anode is limited by the gold plane and anode geometry, not the screens. Therefore, the aperture of the screens are acceptably over-sized because the possible off-nominal position of the screen will not affect data acquisition. The main aperture of the housing matches the screen aperture dimensions of 1.150" by 0.950" with filleted corners.

In addition to the rectangular pocket for the screens, there is an additional pocket to make clearance for the tab in the sweep screen as shown in Figure 3.7. In previous versions, the wiring connecting the screens and preamp board was exposed which created an exposed voltage on the outside of the sensor. In order to enclose all of the wiring, I extended the total size of the housing to enclose the electronics. Because all the wiring connecting the screens to the preamp board is on one end of the PIP, extending the housing only on this side made the PIP asymmetrical. However, completely enclosing the electronics and minimizing the PIP mass justify the negative consequences of a slight asymmetry.

The top housing has several holes for different purposes (Figure 3.7). There are four #4 clearance holes on the corners to screw the top housing down to the brass piece. There are also four tapped #0-80 holes to attach the gold planes to the top of the PIPs. A gold

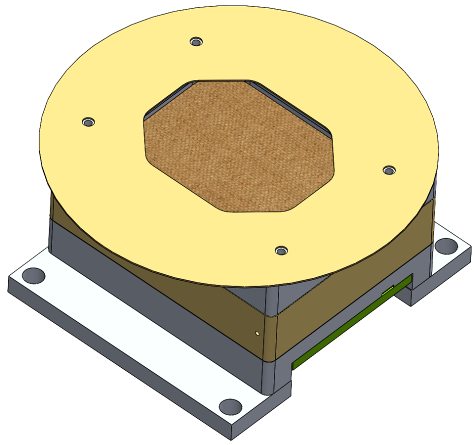

Figure 3.9: Gold plane mounted to the top of a PIP on the main payload. The gold plane is 2.25" in diameter.

plane is shown mounted to the PIP in Figure 3.9. These holes are symmetrically located from the center of the aperture, not the middle of the PIP in order to make the gold planes symmetrical along both central axes. The gold planes are installed later on in the integration process. Until then, plastic covers are mounted on top of the PIPs to prevent any damage to the screens during integration. There are two additional #0-80 tapped screw holes for these plastic covers. Even after the gold planes are installed, the plastic covers are taped to the top of the gold planes, as seen in Figure 3.1, to protect the screens until the final steps leading up to launch.

The top housing is made from aluminum because it is cheap, readily available, lightweight, and conductive. Therefore, we can maintain the housing at the ground voltage.

3.3 Gold Planes

The main purpose of the gold planes is to make the electric field perpendicular to the PIP aperture over a relatively large area. Gold can do this because it is a conductor. In electrostatics, if a conductor has a net charge, the charges reside on the surface of the volume and produce an electric field perpendicular to said surface [2]. The collimated electric field

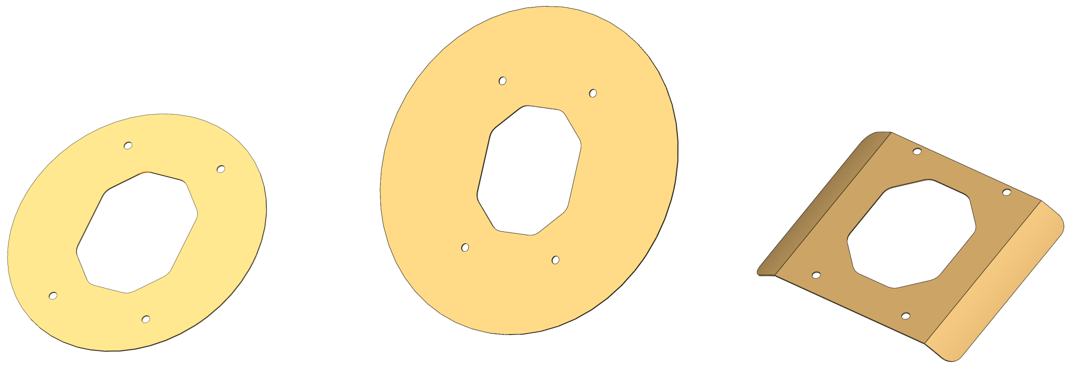

Figure 3.10: Gold planes for PIPs at different locations. The main payload gold planes (left) are 2.25" in diameter. The Bob forward PIP gold planes (middle) are 2.875" in diameter. The Bob side PIP gold planes (right) are 1.7" in length. Each gold plane has the same aperture defined by the anode and the same four #0 clearance holes for mounting.

aids in accelerating the ions perpendicularly into the anode which is ideal for data acquisition. Without the gold planes, the ions would be more likely to enter the PIP at an angle [11]. Although there are less expensive conductive materials, gold was chosen because it does not form an oxide layer on its surface, which would disturb the electric field.

Each gold plane is a thin piece of nickel substrate with gold plating. The gold plane stock material is very costly. It was important to maximize the effect of the gold plane while minimizing the cost (see Appendix D). Each gold plane has an anode-matching aperture and corresponding #0 mounting holes. Different PIPs have different gold plane sizes, as shown in Figure 3.10, based on their location on the main payload or Bob. The main payload PIPs have circular planes with a 2.25" diameter. The Bob forward gold planes are also circular and are 2.875" in diameter. The Bob side gold planes have a rectangular shape, are 1.7" in length. They are curved on two ends to match the radius of the Bobs.

3.4 Brass Piece Design

The brass piece, shown in Figure 3.11, serves two main purposes. Firstly, it defines the distance between the top ground screen and the anode. Secondly, it reestablishes the gold

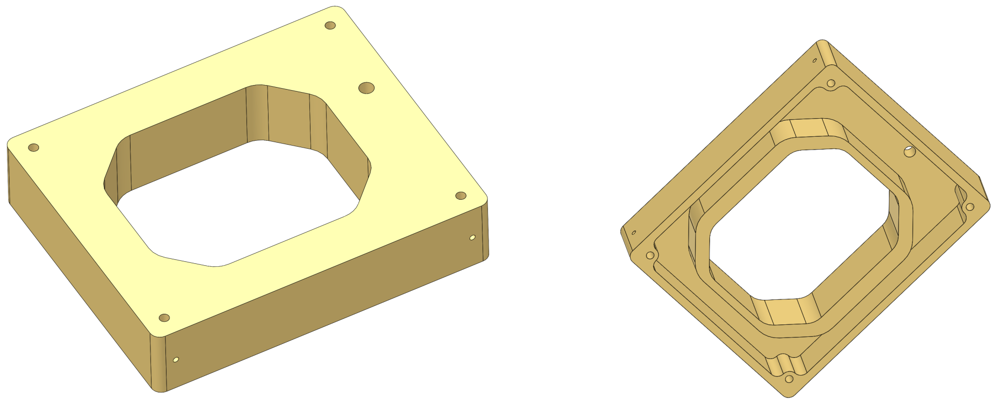

Figure 3.11: Brass piece view from above (left) and below (right). The outer dimensions of the housing are 1.4" by 1.7".

plane aperture. It also includes four tapped #4-40 holes so the top housing and bottom housing can be clamped to it. Each tapped hole is used by two screws, one from the top clamping the top housing, and one from the bottom clamping the bottom housing. This efficient use of tapped holes creates an opportunity for air to get trapped. To account for this, each of these tapped holes has a vent hole at its midpoint. The brass piece also has a clearance hole for the metal pin extending down from the sweep screen tab to the preamp board as mentioned in the screen section.

During the first iterations of the brass piece, it contributed 63% of the total PIP mass. To save mass, I decided to remove all unnecessary mass in the brass piece. I added a pocket in the underside, maintaining a wall around the outside, tapped holes, and the inner aperture, as seen in the right image of Figure 3.12. This feature decreased the brass piece mass from 0.072 kg to 0.043 kg. The current brass piece contributes 51% of the total PIP mass. Although this is a high percentage, brass's material properties justify the mass contribution. Brass was chosen because it does not oxidize as much as aluminum. This matters because the interior wall of the brass piece forms the walls of the region where the ions travel between the screens.

Although this mass-removal feature was necessary, it introduced thin wall thickness into

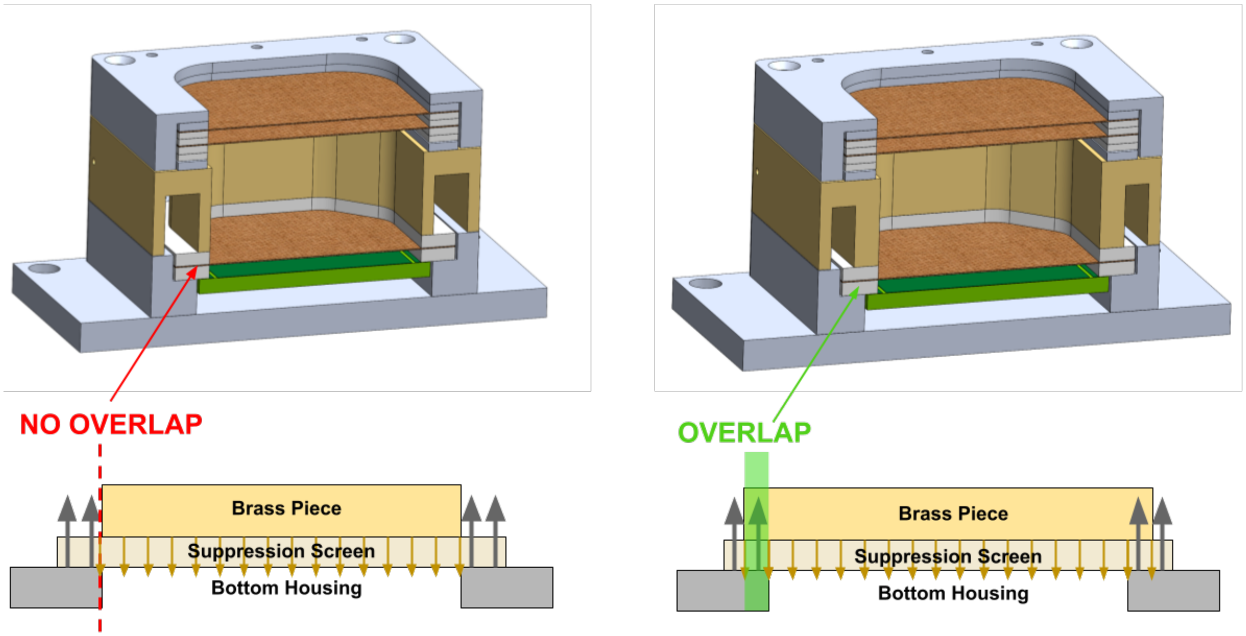

Figure 3.12: PIP brass piece with no extended inner walls (left). PIP brass piece with extended inner walls (right). The overlap allows the suppression screen to be supported around the entire perimeter. Only the long edges of the brass piece aperture walls are thickened in this way. The downward force from the brass piece (dark yellow) is from the entire inner aperture of the brass piece, including the short, non-thickened sides balances the upward force from the bottom housing (gray).

the design. The inner wall is the only area that the suppression screen presses up against when it is clamped, so it is important to maintain enough thickness for a sufficient clamping area. The long edges of the inner aperture wall of the brass piece were thickened to ensure overlap between the contact of the brass piece and the bottom housing on the suppression screen, as shown in Figure 3.12. This also reduces risk of bending in the suppression screen. Without overlap, the deflection can be modeled as a beam with two pivoting ends with a uniform weight distribution. The overlap will better support the suppression screen, minimizing deflection.

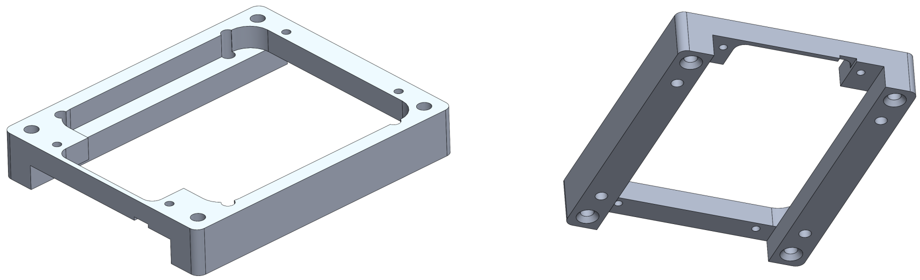

Figure 3.13: PIP bottom housing view from above (left) and below (right). The outer dimensions of the housing are 1.4" by 1.7".

3.5 Bottom Housing Design

The aluminum bottom housing, shown in Figure 3.13, has several features that are similar to the top housing. Firstly, it has a pocket for the suppression screen with the same sizing justifications as the top housing. In previous designs, the suppression screen was smaller in area than the ground and sweep screens. All of the screens were conveniently changed to have the same outer dimensions for the GNEISS mission. There are the same four #4 clearance holes on the corners of the bottom housing to screw the bottom housing up to the brass piece. In addition, there are four tapped #0-80 holes to secure the preamp board, which includes the anode, into place. The preamp board is screwed onto the underside of the bottom housing. The bottom housing is configured so that the suppression screen is flush with the preamp board when the PIP is assembled. I made a pocket, an extension of the screen pocket, in the bottom housing to make space for both the tab in the suppression screen and all of the pads and soldered connections on the preamp board. This cutout is just large enough to not make electrical contact with the pads while maintaining a sufficient 0.050" wall thickness. There is also a small cutout to make room for a wire bundle exiting the preamp board.

The bottom housing feet are tall enough to make sure that there is enough room for the solder and wiring on the preamp board, as seen in Figure 3.14. On the bottom of the housing, there are four #2-56 tapped holes for the base plate to be mounted to the PIP. The

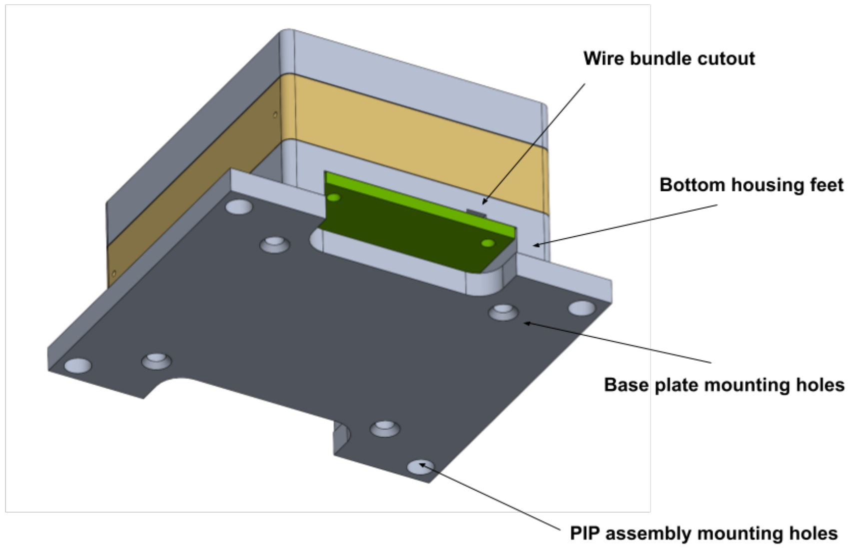

Figure 3.14: PIP underside view with base plate. The base plate includes countersinks to ensure that the flathead screws mounting the base plate are flush.

base plate is shown mounted to the PIP bottom housing in Figure 3.14.

3.6 Base Plate Design

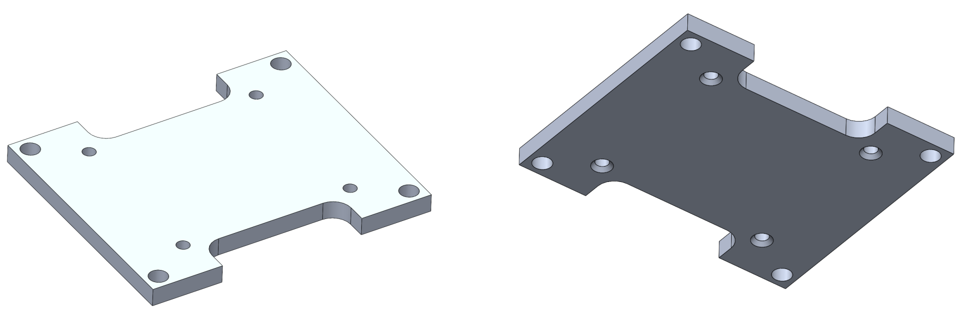

Figure 3.15: PIP base plate view from above (left) and below (right). The outer dimensions of the base plate are 1.7” by 2”.

The aluminum base plate, shown in Figure 3.15, is used to easily attach the PIPs to the main payload PIP trees and the Bobs. It has four #2 clearance holes with countersinks that attach the base plate to the bottom PIP housing. The countersinks are on the bottom side of the base plate so the screw heads do not protrude, allowing the bottom side of the base plate to be flush with the surface it is mounted to. This feature makes it possible to mount the PIPs from the top or bottom of the base plate — a key design feature for the Bobs. Additionally, there are two symmetrical cutouts in the base plate to allow extra room for wires to exit the bottom side of the anode. These cutouts also allow for clear preamp board visibility. Each of the boards will be individually labeled to differentiate them. The cutouts will allow us to easily see the label to identify the different PIPs during testing and integration.

As of March 2025, all of the PIP parts, including the top housing, brass piece, bottom housing, and the base plate, have been machined and cleaned. Once the screens stacks and preamp boards are ready, the PIPs will be assembled. In December, we tested an earlier iteration of the PIP which included the new top housing and bottom housing acting as clamps for the screens. The PIP passed all electrical tests, proving that the new PIP design could preform all necessary tasks during the GNEISS mission. Since then, only small mechanical changes have been made. Compared to previous PIP fabrication cadences, my changes to the mechanical PIP structure and screen fabrication processes resulted in a 75% decrease in labor time. Therefore, I have significantly improved the PIP manufacturing and fabrication processes while maintaining the PIP's function.

Chapter 4

Bobs

Bobs are ejectable subpayloads that use PIPs to gather data away from the main payload trajectories. The Bobs are ejected through rifled tubes located on the main payloads. When they are ejected, they are pushed out of their tubes with springs, giving them an angular velocity ω. Ideally, the angular velocity would correspond to the main axis of the rifled tube. Unfortunately, the mechanics of the rifled tubes apply an asymmetric torque, called a "tip-off torque," to one end of the Bob as it exits the payload. This causes the Bob to exhibit coning as it travels away from the main payload in free fall [12] [15].[1] Although this motion is not ideal, it is unavoidable with the current technology and resources available.

To account for the Bob's imperfect motion, calibrated magnetometers are used to determine the location and orientation of the Bobs [15]. One of the assumptions when calibrating the orientation of the Bobs is that they have a diagonalized inertia tensor when the body axis (the axis along the center of its cylindrical shape) of the Bob is a principal axis [15]. This diagonalized inertia tensor would cause a Bob to not cone at all if there were no tip-off torque, making the angular velocity parallel to the angular momentum.

If the Bob's location, the Bob's orientation, and the ion flux through each of the PIPs

[1]Previous Bobs from the Isinglass mission experienced coning with half angles: 31°, 12°, 25°, 6°, and 7° [16]. This Bob design, developed by Prof. Kristina Lynch and Dr. Rob Clayton was also used for the Kinet-X mission. For the sake of simplicity, I will refer to this Bob design as the "Isinglass Bob" or the "old Bob."

are known, the velocity of the ionospheric plasma can be calculated, which is one of the ultimate goals of the GNEISS mission. In order to accurately determine the velocity of the ionospheric plasma, the inertia tensor must be diagonalized within uncertainty.

4.1 Bob Overview

The structure of the Bob is divided into two sections. The back end of the Bob is engineered by NSROC. This side interacts with the rifled tube in the main payload and contains a power supply and various telemetry elements [6]. This end of the Bob is uniform across NSROC missions. The front end of the Bob, which contains our PIPs, is specific to our mission and is the side that I am designing. A closeout plate serves as an adapter between the front and back ends of the Bob. This plate has holes for D-sub connectors and other necessary electrical connections between the sides of the Bob. For the sake of simplicity, I will refer to mission-specific front end of the Bob as "Bob."

The outer geometry of the Bob is defined by NSROC and is uniform across missions. This is essential because it must comply with the predetermined dimensions of the rifled tube from which it is ejected. All components, including the gold planes, must reside within the defined profile to guarantee a successful ejection.

Six total Bobs will be made for the GNEISS mission which calls for a Bob with two PIPs, as shown in Figure 4.1. One PIP faces forward and the other faces radially outward, similarly to the PIP configuration on the Isinglass mission launched in 2017 [15]. The exterior of the Isinglass Bob is shown in Figure 4.2. The Isinglass mission identified opportunities for mechanical improvements for the Bob.

4.2 Bob Coning

Coning appears as wobbling during flight. While coning, the Bob will sweep a cone-like shape with its central axis as it travels. This occurs when the angular velocity vector $\boldsymbol{\omega}$ is

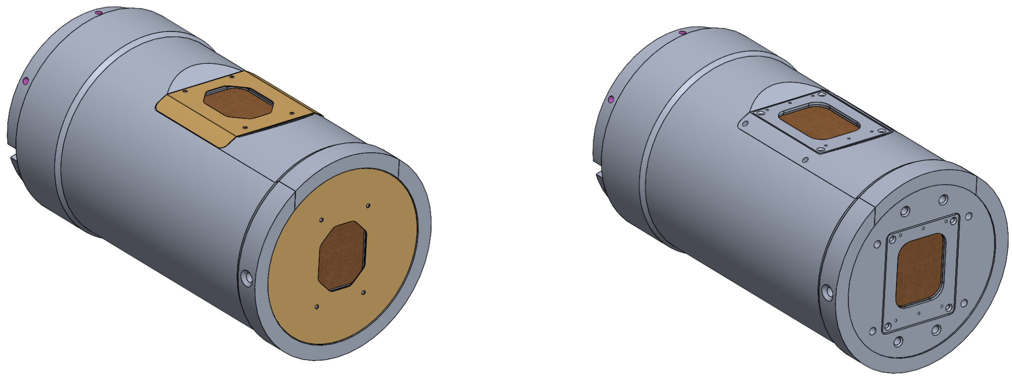

Figure 4.1: Bob with all components and gold planes (left). Bob without gold planes to highlight location of PIPs (right). There is one PIP on the forward end of the Bob and one PIP on the side facing radially outward. The Bob is mission-specific and is 6.225" long.

not parallel with the angular momentum vector $\boldsymbol{L}$ [17].

$$\boldsymbol{L} = \boldsymbol{I}\boldsymbol{\omega} \tag{4.1}$$

These values are related by the inertia tensor $\boldsymbol{I}$ [17].

$$\boldsymbol{I} = \begin{pmatrix} I_{xx} & I_{xy} & I_{xz} \\ I_{yx} & I_{yy} & I_{yz} \\ I_{zx} & I_{zy} & I_{zz} \end{pmatrix} \tag{4.2}$$

In this tensor, there are three moments of inertia: I_{xx}, I_{yy}, and I_{zz}. These are the moments of inertia about the x-, y-, and z-axes respectively. The moment of inertia about an axis is the sum of each infinitesimal mass m_α multiplied by its distance from the axis r_α squared [17].

$$\boldsymbol{I_x} = \sum m_\alpha r_\alpha^2 \tag{4.3}$$

There are also six products of inertia in the inertia tensor: I_{xy}, I_{yx}, I_{yz}, I_{zy}, I_{zx}, and I_{xz}. Consider a point mass, as described by Figure 4.3, rotating about the z-axis at a fixed

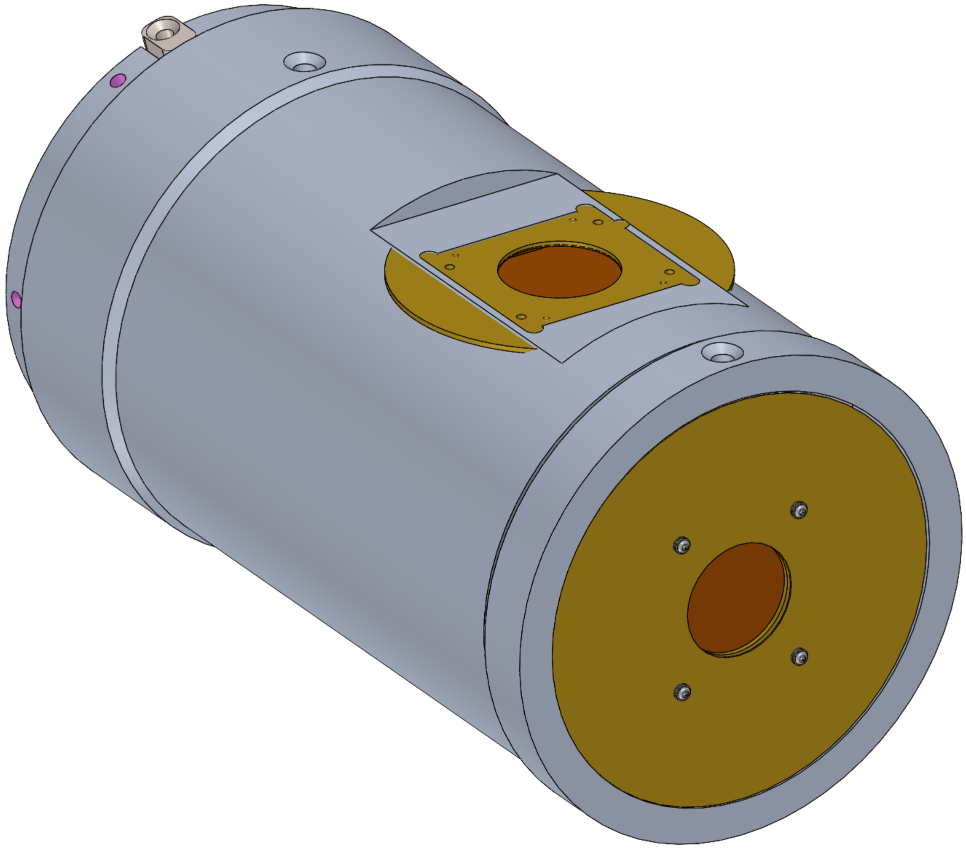

Figure 4.2: Isinglass Bob exterior. The Isinglass Bobs, similarly to the GNEISS Bobs, contain one forward PIP and one side PIP.

radius r_z at a constant distance r_x from the x-y plane. When the point mass crosses the x-z plane, its instantaneous velocity only has a component parallel to the y-axis. At this instant, the point mass has a nonzero angular momentum about the x-axis because it has a velocity with a component perpendicular to the x-axis at a distance r_x. This angular momentum is taken into account with the product of inertia which is equal to the negative sum of each infinitesimal mass m_α multiplied by its distance(z_α) from the axis about which it rotates (the z-axis) and the distance (x_α) from a chosen perpendicular axis (the x-axis) [17].

$$\boldsymbol{I_{xz}} = -\sum m_\alpha x_\alpha z_\alpha \tag{4.4}$$

Coning is minimized when the angular momentum vector is parallel to the angular velocity vector and aligned to a principal axis. This is achieved by manipulating the inertia tensor via mechanical design in a process called diagonalizing the inertia tensor. The inertia tensor is diagonalized when all of the products of inertia are equal to zero. When looking at the equation for products of inertia in the context of the Bob, it is clear that each infinitesimal mass cannot equal zero nor can the distances from the axes. However, we can take advantage of symmetry in the mechanical design to achieve near-zero products of inertia.

Consider a Bob composed of two equal point masses at the same y and z coordinates relative to the center of mass but at opposite x coordinates. Looking at the product of inertia $\boldsymbol{I_{xz}}$:

$$\boldsymbol{I_{xz}} = -\sum m_\alpha x_\alpha z_\alpha = -(mxz + m(-x)z) = 0 \tag{4.5}$$

The product of inertia equation reveals that using mass symmetries will diagonalize the inertia tensor.

Every body has a set of three perpendicular axes which diagonalize the inertia tensor. These are called the principal axes. When a body rotates about one of its principal axes, the angular momentum and angular velocity vectors are parallel. In the case of the Bob, its intended rotation is about its body axis only. Therefore, its principal axes should be made to be its body axis and any two additional perpendicular axes by implementing mass symmetries.

As previously mentioned, this would be the ideal case. Bob coning is inevitable due to the unpredictable tip-off torque. However, a diagonalized inertia tensor with the Bob body axis as a principal axis is still desirable is because it is an assumption in the Bob's orientation calibration procedure [15].

I implemented the concept of mass symmetries to achieve the following inertia tensor using the Bob's body axis as a principal axis (the z-axis in Figure 4.4) and two additional perpendicular axes (the x-axis and y-axis in Figure 4.4). The inertia tensor was calculated

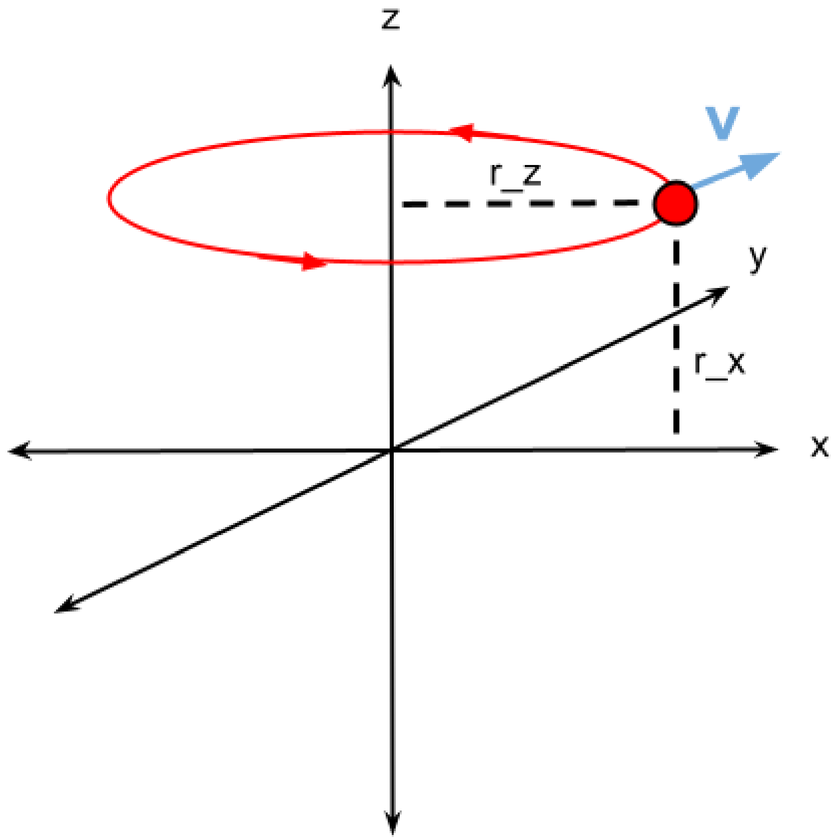

Figure 4.3: A point mass rotating about the z-axis at a constant radius r_z at a constant distance r_x from the x-y plane. At the instant shown in the figure, the point mass has an instantaneous velocity $\boldsymbol{v}$ which is parallel to the y-axis.

using SolidWorks 2024.

$$\boldsymbol{I_{GNEISS}} = \begin{pmatrix} 2726.15 & 0.97 & -1.96 \\ 0.97 & 2791.16 & 0.23 \\ -1.96 & 0.23 & 1148.45 \end{pmatrix} kg(mm)^2 \tag{4.6}$$

For comparison, the Isinglass Bob design gives the following inertia tensor.

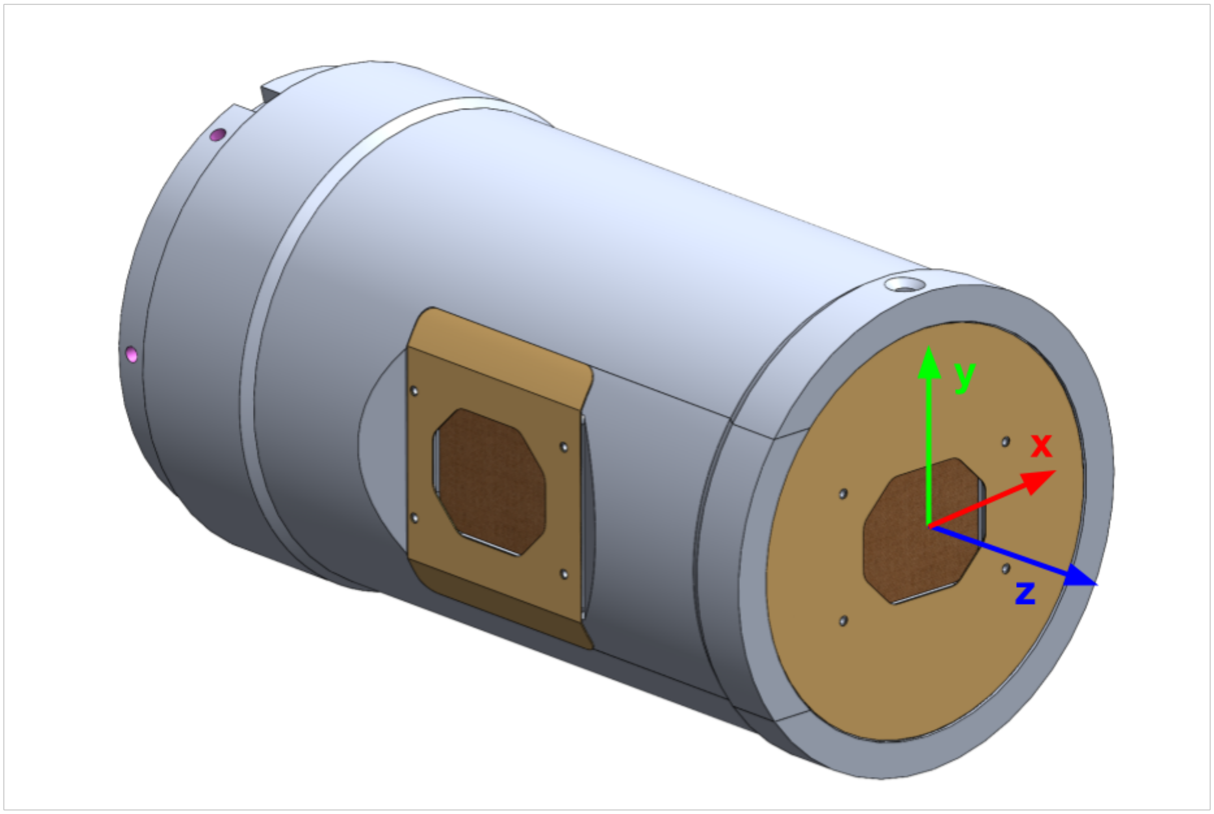

Figure 4.4: Bob with labels to specify axes. The primary rotational symmetry axis of the Bob is the z-axis.

$$\boldsymbol{I_{ISINGLASS}} = \begin{pmatrix} 2920.53 & -1.64 & -3.57 \\ -1.64 & 2855.32 & 4.14 \\ -3.57 & 4.14 & 1128.39 \end{pmatrix} kg(mm)^2 \tag{4.7}$$

While the moments of inertia are similar, the new Bob design boasts products of inertia that are slightly smaller than those of the old Bob design. In contrast, the current NSROC back end of the Bob gives the following inertia tensor.

$$\boldsymbol{I_{NSROC}} = \begin{pmatrix} 3447.95 & 22.32 & 42.93 \\ 22.32 & 3197.68 & -12.03 \\ 42.93 & -12.03 & 1236.98 \end{pmatrix} kg(mm)^2 \tag{4.8}$$

To give these inertia tensors context, a typical $\frac{1}{2}$" #6-32 stainless steel screw weighs approximately 0.001 kg.[2] If this screw is placed in the tapped hole located on the edge of the Bob enclosure directly above the forward PIP aperture in Figure 4.4, it will be approximately 37 mm away from the center of mass along the y-axis and 58 mm away from the center of mass along the z-axis. Using Equation 4.5, we can calculate that the screw's contribution to the product of inertia $\boldsymbol{I_{yz}}$ is 2.15 kg·mm^2.

When comparing the screw's contribution to the inertia tensor to the new Bob design's inertia tensor, it becomes apparent that each product of inertia is within one screw's contribution of zero. There is still uncertainty in the inertia tensor calculated from the model because there are components in the real Bob that are not included in the SolidWorks model, such as wires, connectors, and small screws, which will make unknown mass contributions. Using the screw's contribution as a metric, the new Bob inertia tensor is only a small improvement compared to the old Bob inertia tensor. However, this slight improvement is commendable considering the new asymmetries in the necessary internal electronics. In addition, the mass distribution of the NSROC side is not under my jurisdiction. Small iterative changes may occur later in its hardware design process, leaving any more changes I make lost in the noise. Given these circumstances, the new Bob design's inertia tensor is diagonalized to an acceptable extent. In the next section, I will describe the design decisions I made to achieve this inertia tensor.

[2] To achieve this estimate, I used a STEP file of a stainless steel $\frac{1}{2}$" $\#6-32$ screw from McMaster-Carr and used SolidWork's 'Mass Properties' feature (see Appendix B).

4.3 Bob Cap

As previously mentioned, the Isinglass mission revealed opportunities for mechanical improvement for the Bob. Firstly, the Bobs' fabrication process was excessively long due to the inefficient side PIP installation process. Additionally, it became apparent that simplifications could be made to the internal electronics.

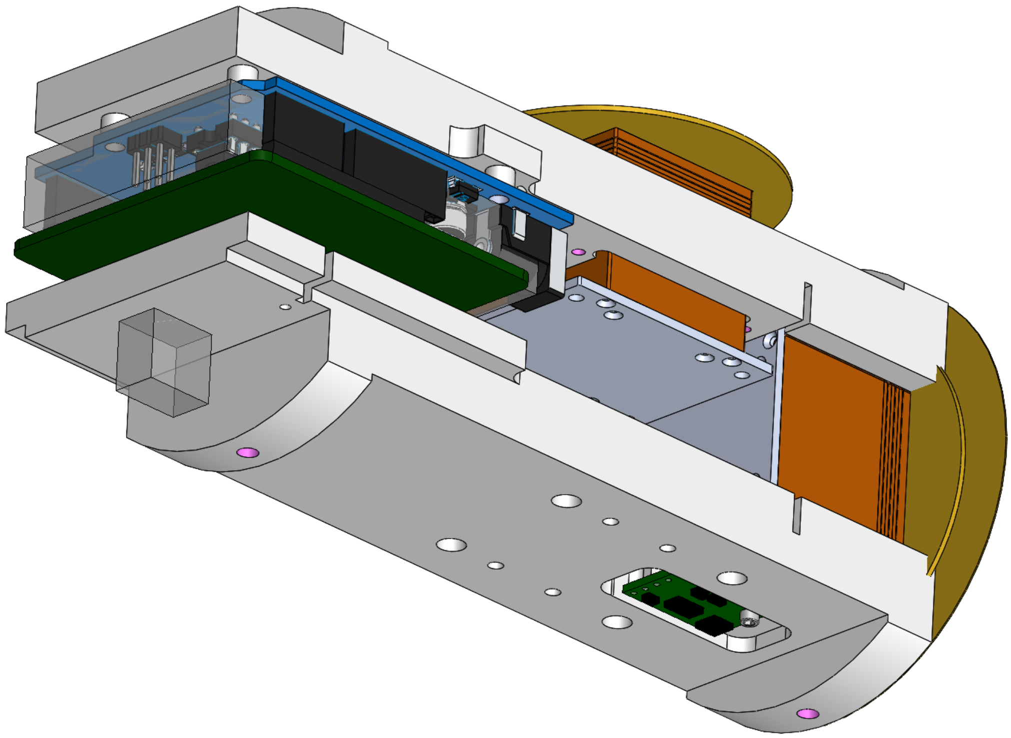

Figure 4.5: Isinglass Bob interior. The Isinglass Bobs contained two PCBs as opposed to the GNEISS Bobs' single PCB[4]: the shield board. This Bob also includes one forward PIP and one side PIP.

Mission-specific design comes into play with the Bob cap. In previous missions where we have had Bobs with one forward facing PIP and one side facing PIP, the fabrication process was suboptimal due to inefficiencies in the mechanical design. In order to insert the side PIP, it had to be inserted along the main body axis of the PIP toward the location of its hole and then pushed out into place in a finicky manner (Figure 4.6). The process of installing

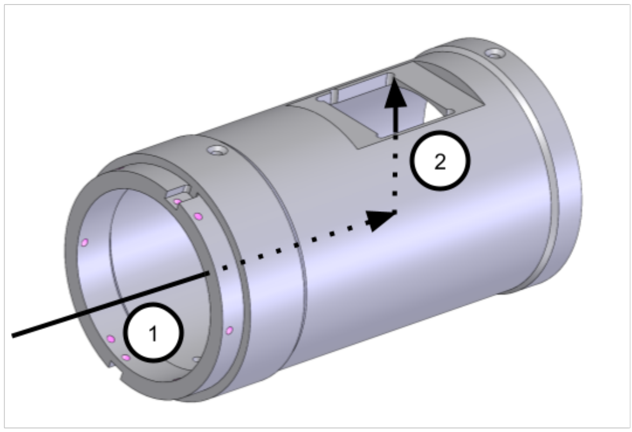

Figure 4.6: Isinglass Bob side PIP installation. Because the side PIP has an enclosed cutout, the side PIP had to be slid along the along axis of the Bob (1) then pushed out radially (2). This tedious process was unideal for the repetitive assembly and disassembly that occurs during testing.

the side PIP and removing it for various tests and troubleshooting added significant labor and time to the testing and fabrication process. In addition, simplifications have been made to the Bob's electrical components. Innovations in the shield board design reduced the total number of PCBs from two to one, as shown in Figure 4.5. Although this is an efficient improvement, it creates another inherent mass asymmetry which must be resolved. I have altered the Bob design to avoid this PIP insertion issue and to accommodate the new PCB configuration.

Instead of inserting each component into the main body of the Bob individually then mounting them, I have created a design that uses a completely removable cap which also serves as housing for all of our electrical components in the Bob, as shown in Figure 4.7. The

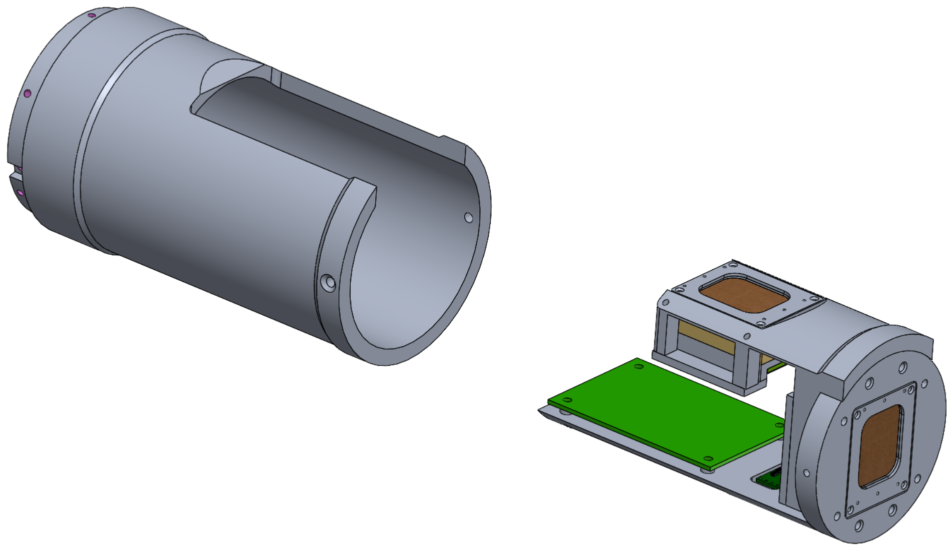

Figure 4.7: Bob with cap removed to show simple removal motion and to reveal internal components.

Bob cap includes the two PIPs, a shield board, and an IMU. Not only is insertion significantly simplified, but all of the hardware can be installed on the cap in its final configuration with full access for testing, as shown in Figure 4.8. When the cap is ready for installation, it can be easily slid into the aluminum Bob enclosure and secured with just three strategically placed screws. This mechanical improvement reduced the Bob assembly time by 50%.

The Bob enclosure and all Bob cap piece will be machined out of aluminum because it is a lightweight, relatively inexpensive, an easily machinable material.

As previously mentioned, much of the Bob enclosure geometry, including the length, radii, and closeout plate mounting holes, is defined by NSROC. Given this constraint, the only mission-specific features I added to the Bob were three clearance holes to mount the Bob cap and a sloped plane next to the side PIP to ensure the enclosure did not block the PIP's field of view. The enclosure has a large slot removed to accommodate the Bob cap. Removing this material from the enclosure is acceptable because the inserted Bob cap contributes the outer Bob geometry defined by NSROC.

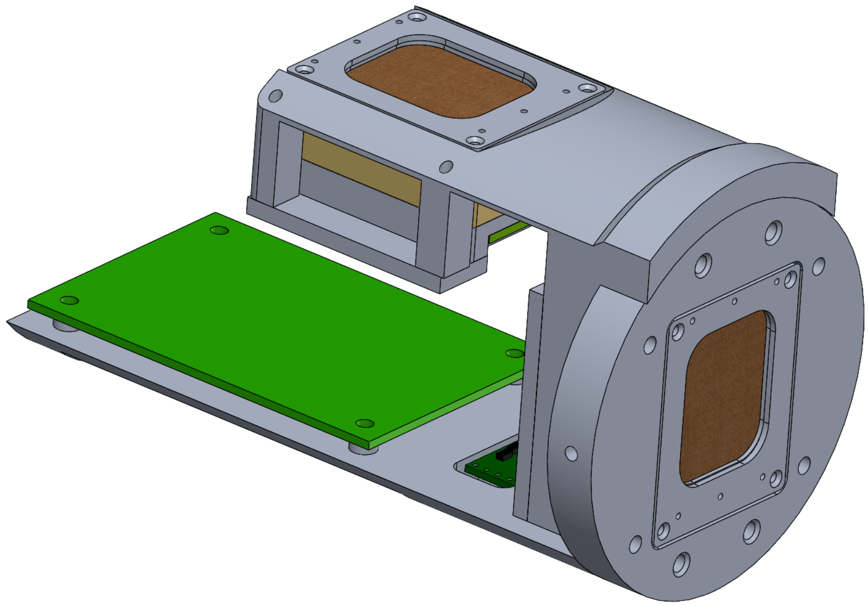

Figure 4.8: Bob cap with components. Two PIPs, a shield board, and an IMU are installed on the Bob cap. On its own, the Bob cap is 5.41” in length.

The Bob cap is separated into three different aluminum parts to make the manufacturing process easier, as shown in Figure 4.9. These parts are: the cap disc, the cap L-bracket, and the cap longeron. The cap L-bracket and cap longeron are each mounted to the cap disc with a pair of $\#4-40$ screws. The parts were separated in this way to minimize the amount of machining labor and initial stock material.

The cap disc serves as the base of the cap design. It is a short cylinder with a rectangular cutout for the forward facing PIP, as shown in Figure 4.10. The cutout is 1.45” by 1.75” to match the PIP profile with 0.0125” of clearance on each side. The cutout is 0.05” off center to account for the asymmetry in the PIP; this way, the aperture is centered on the long axis of the Bob. Recall that the anode in the PIP is 0.050” off center with respect to the outer profile of the PIP to completely enclose the PIP wiring. The cap disc contains four $\#4-40$ clearance holes in its front face to mount the cap L-bracket and longeron pieces. These holes have deep countersinks to keep the mounting screws below the front plane of the

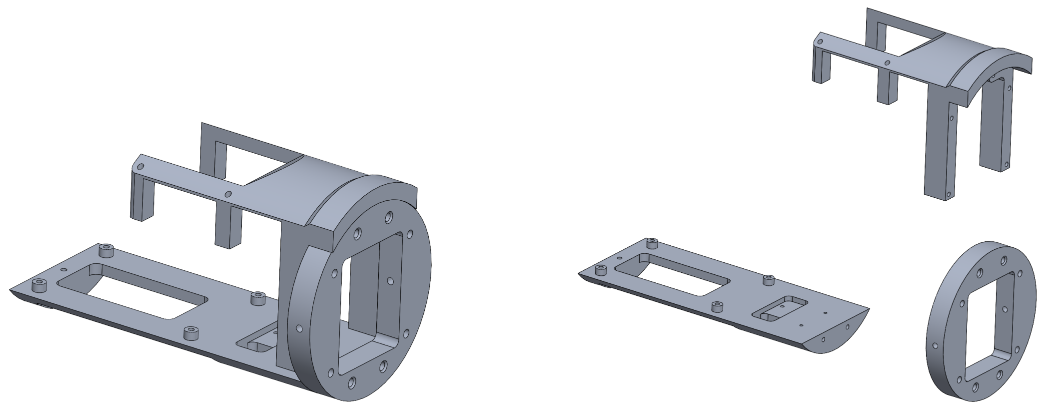

Figure 4.9: Bob cap without components (left) and corresponding exploded view (right). There are three parts that make up the Bob cap. The Bob cap L-bracket (top) and the Bob cap longeron (bottom) are both mounted onto the Bob cap disc.

Bob, allowing the Bob forward gold plane to also be flush. There are also four #4 clearance holes to serve as vent holes for the forward PIP mounting holes in the cap L-bracket. There are two tapped $\#6-32$ holes on the sides of the cap disc that are 180° away from each other. These holes, used to secure the Bob cap to the Bob enclosure, will be drilled from the outer diameter of the disc through to the rectangular hole to allow for venting. There is space for venting because of the extra 0.0125" of clearance around the cutout for the PIP.

The L-bracket piece, shown in Figure 4.11, is mounted directly to the back of the cap disc. The upper geometry of the L-bracket piece is defined by the Bob profile decided by NSROC. There are two rectangular cutouts, one for each of the PIPs. Each of these cutouts is sized to match the PIP profile, similar to the hole in the cap disc but with one open end with 0.0125" of clearance on each side. Each of the two cutouts are surrounded by two arms. The top side of the PIPs' base plates are mounted to these arms which have tapped $\#4-40$ holes, matching the locations of the clearance holes in the PIP base plate. The arms are just tall enough to make the top plane of the PIP top housing flush with either the cap disc or the outer side of the L-bracket.

Over iterations of the cap L-bracket, I removed a significant amount of mass, especially

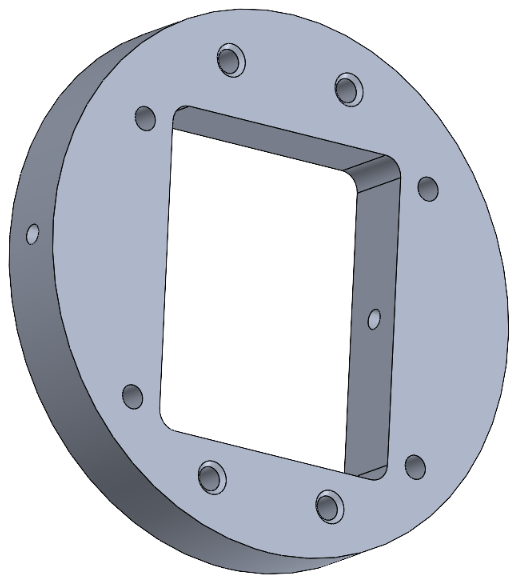

Figure 4.10: Bob cap disc. It is 2.9” in diameter.

surrounding the side PIP cutout in efforts to diagonalize the inertia tensor. This area was an ideal location for mass-removal because it is relatively radially far from the center of mass, which has a larger contribution to the product of inertia per infinitesimal mass according to Equation 4.5. Additionally, removing mass from the L-bracket around the side PIP countered the product of inertia contribution of the side PIP, an inherent mass asymmetry in the Bob.

The cap longeron is also directly mounted to the cap disc. The cap longeron, shown in Figure 4.12, houses both the shield board and an IMU. Additionally, it serves as a counter-mass for the side PIP to aid in improving the Bob’s mass distribution. I have included two tapped $\#4-40$ holes with corresponding vent holes in the Bob longeron to mount it to the cap disc. There is also a tapped $\#4-40$ in the opposite end of the longeron to secure the other end of the cap longeron to the Bob enclosure. The top face of the longeron has four 0.125” tall bosses, with $\#4-40$ tapped holes, which are spaced to match the mounting hole locations of the shield boards. Mass has been removed under the shield board in efforts to precisely distribute mass in the longeron.

There is also a pocket in the cap longeron to house the IMU. The IMU is a commercially

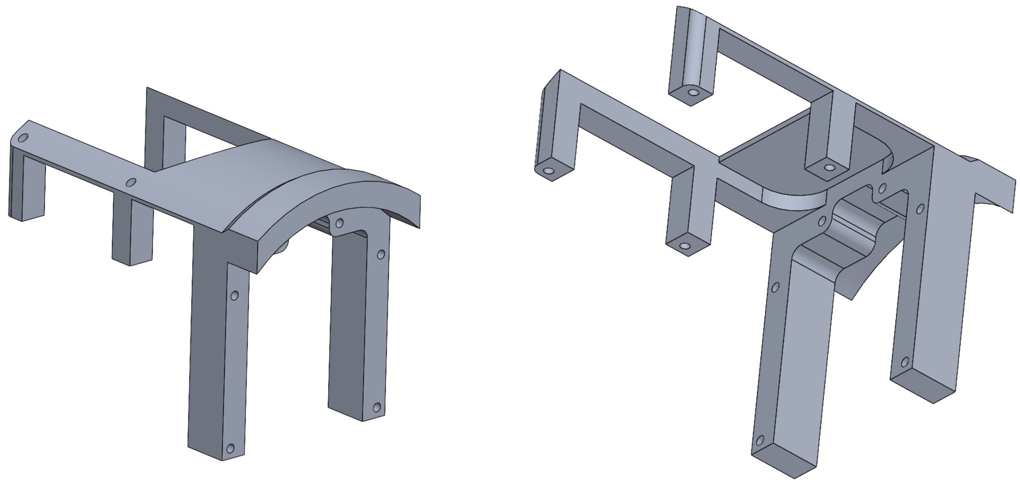

Figure 4.11: Bob cap L-bracket top view (left) and bottom view (right). Significant mass-removal features can be see in the underside of the L-bracket around the side PIP cutout. The L-bracket is 3.5" in length.

available PCB which measures the acceleration, magnetic field, and angular velocity along three perpendicular axes. The IMU is essential to the Bob's function because its collected data is used to locate and orient the Bob [15]. In order to relate these values accurately to the Bob's orientation, it is important that the IMU is physically constrained. The IMU will be aligned to the long edges of the IMU pocket and further constrained by a screw securing it to the tapped $\#2-56$ hole in said pocket. The underside of the IMU is electrically conductive but only on one end. I made an additional deep pocket below these conductive components to prevent them from touching the conductive cap longeron. This deep pocket also provides a space for wires to exit the underside of the IMU.

The placement of the cap longeron helped create necessary mass symmetries to diagonalize the Bob's inertia tensor. This spatial solution neatly uses both inherent mass asymmetries to counteract each other. By placing the cap longeron and shield board opposite the side PIP, the infinitesimal masses at near-maximum radial distances from the center of mass cancel out, similar to the two-point-mass example given in the Bob coning section.

An additional benefit of this new Bob design is the decrease in mass. The new design

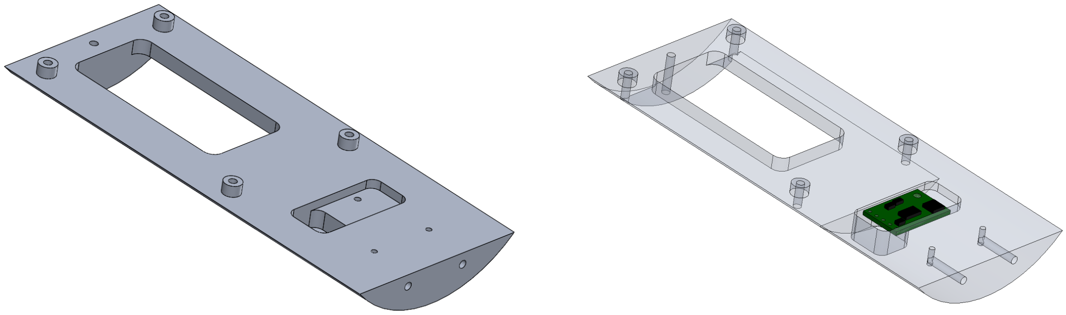

Figure 4.12: Bob cap longeron (left). The longeron is made transparent in the figure to clearly display the IMU pocket to make room for electrical connections (right). The longeron is 5” in length.

decreased the mass of the Bob front end from 0.99 kg to 0.92 kg. The NSROC end of the Bob still weighs 1.17 kg. With the new Bob front end, the total Bob mass decreases by 3.2%. Lightening the payload where possible is always good practice. Moreover, assuming the ejection spring potential energy is constant and friction and drag are negligible, the initial velocity of the Bob will be greater by 1.6% due to conservation of energy. This allows the Bob to travel slightly farther after ejection due to an increased initial horizontal velocity. By increasing the range of the Bob, ionospheric data at distances farther from the main payload trajectories can be collected.

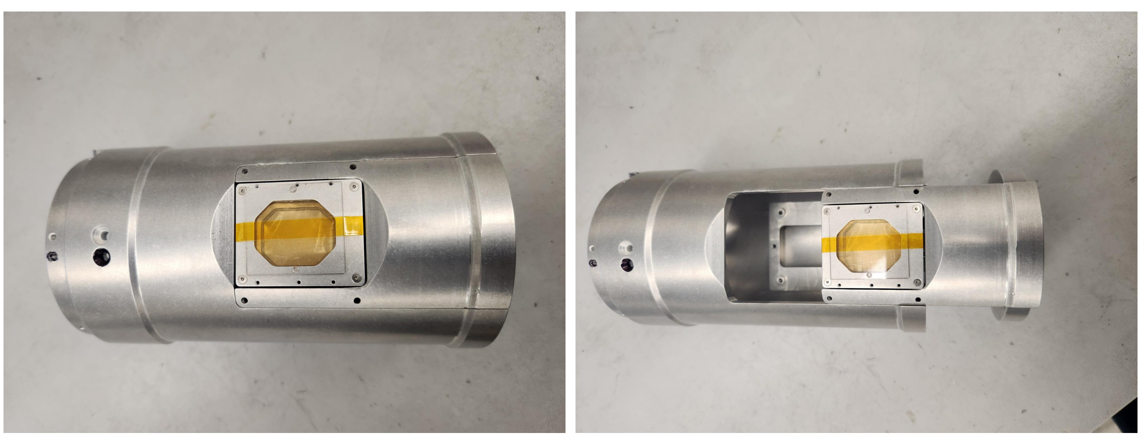

Figure 4.13: Machined Bob with installed PIPs. This sequence shows the Bob cap removal process. This machined Bob reflects a previous iteration of the new Bob design. Additional mass-removal features have been made since. Photos courtesy of Jeffery Renk.

As of April 15th, 2025, a previous iteration of the new Bob design has been machined (Figure 4.13). As of April 16th, the next iteration of Bobs are being machined. These minor changes are reflected by the design described in this chapter.

Chapter 5

Supporting Hardware

Aside from the PIPs and Bobs, I have designed several pieces of supporting hardware for the GNEISS mission. PIP trees are used to position the PIPs on the main payload decks at specified elevation angles. The shield board boxes house shield boards, which electrically control and query the PIPs. The Lattice boxes house components that transmit an RF signal from the main payloads.

5.1 PIP Trees

The goal for the main payload PIPs is to detect the ion flux at the location of the rocket. Fortunately, the rocket spins along its main axis during flight. This allows the PIPs to sweep their field of view azimuthally. The PIPs still need to 'see' 180° from the forward to aft end of the rocket[1]. Each PIP has a half angle view of approximately 20° [16] . To have visibility at all angles, we will place eight PIPs on each rocket at various elevation angles. From the perpendicular axis, there will be one PIP at 75°, 60°, 30°, -30°, -60°, and -90°, and two PIPs at 0°.

There are two decks on the sounding rocket, one on the forward end and one on the aft end. The forward end deck has PIPs at 75°, 60°, 30°, and 0°, and the aft end deck has PIPs

[1]This is almost true. The exciting exception will be discussed later.

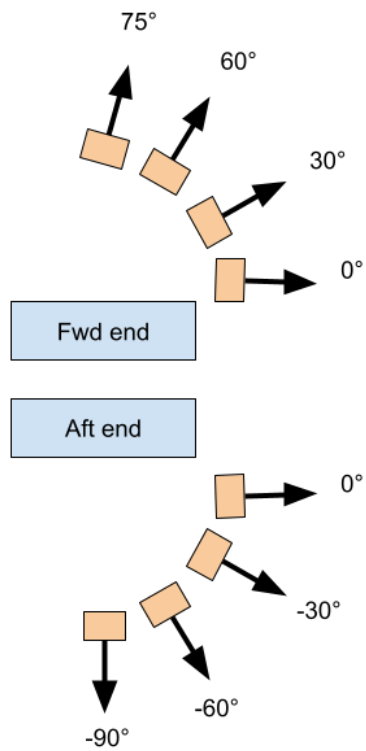

Figure 5.1: PIP elevation angles on each sounding rocket. There are four PIPs at different elevation angles on each deck. The deck on the forward end has PIPs at elevation angles 75°, 60°, 30°, and 0°. The deck on the aft end has PIPs at elevation angles $-90°$, $-60°$, $-30°$, and 0°.

at 0°, -30°, -60°, and -90°, as shown in Figure 5.1. Therefore, the PIP configurations are essentially mirrors of each other with the exception of the PIPs at 75° and -90°. Simulations show that a PIP at a 90° elevation angle (facing directly forward on the rocket) will not provide relevant information. The ion flux we are trying to measure will only be seen in the ram-facing direction. After a main payload maneuver at the beginning of the rocket's trajectory, the body of the rocket will be antiparallel to Earth's magnetic field as shown in Figure 5.3. The velocity (ram) vector is parallel to the trajectory. Therefore, there should be no ion flux into the upleg long axis of the rockets after the maneuver since the rocket is

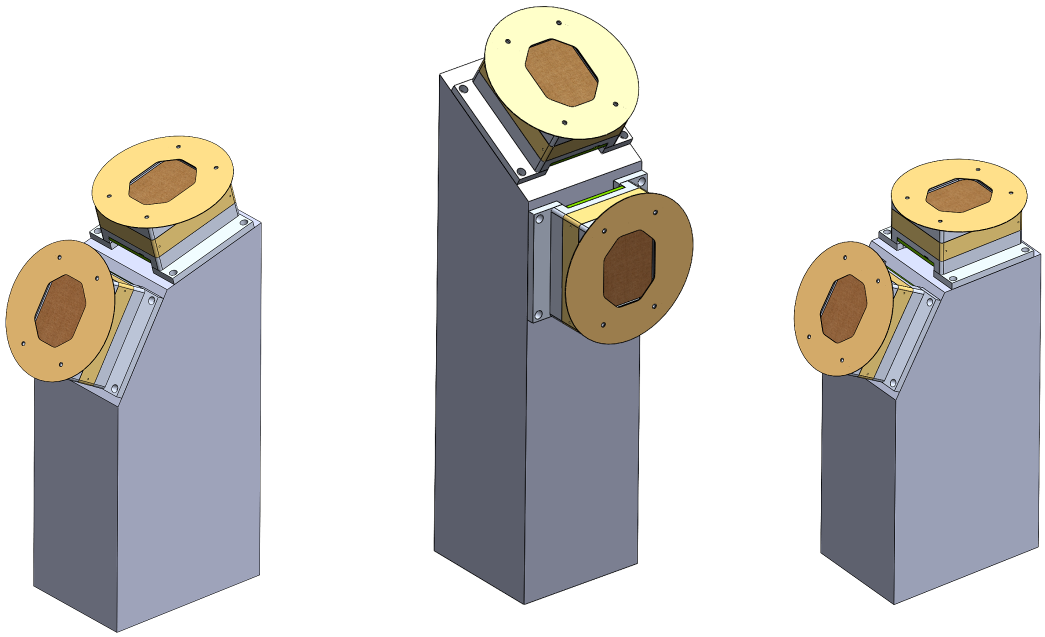

Figure 5.2: PIP trees. PIP tree with elevation angles 75° and 30° (left). PIP tree with elevation angles 60° and 0° (middle). PIP tree with elevation angles -30° and -90° (right). This PIP tree will be mounted upside down on the aft deck. The height of each PIP tree depends on the included elevation angles. They are all approximately 6” tall.

not moving parallel to its axis. This renders the PIP facing forward on the rocket (at 90°) useless. Instead, this PIP is angled at 75° to collect data in a useful direction. The PIP facing the aft end (at -90°), however, still contributes useful data. It is possible for the PIP at -90° to obtain useful ion flux data because it runs into the ions head-on at the end of the rocket's trajectory. The rest of the PIPs are still able to collect ion flux because the velocities of the rockets and the ions are comparable. In this case, the ions run into the rocket.[2]

Each deck includes two different PIP trees, making eight total PIP trees for the GNEISS

[2]Another way to think about ram direction and comparable velocities is with the following thought exercise. Imagine you are driving down a straight highway. Suddenly, you see a large swarm of bugs flying ahead of you. Amazingly, they are moving at approximately the same speed (thermally) as your car! As you and the swarm collide, dead bugs begin to hit your car, completely covering your front windshield (your car's ram direction) and partially covering the side doors and roof. These dead bugs are analogous to measured ion flux. By observing the dead bugs on your front windshield are evidence of your forward motion into the swarm. Because the bugs had some speed as the buzzing around in the swarm, some of them would have hit the sides and top of your car as you drove through. However, there was no way for the swarm to hit your back windshield.

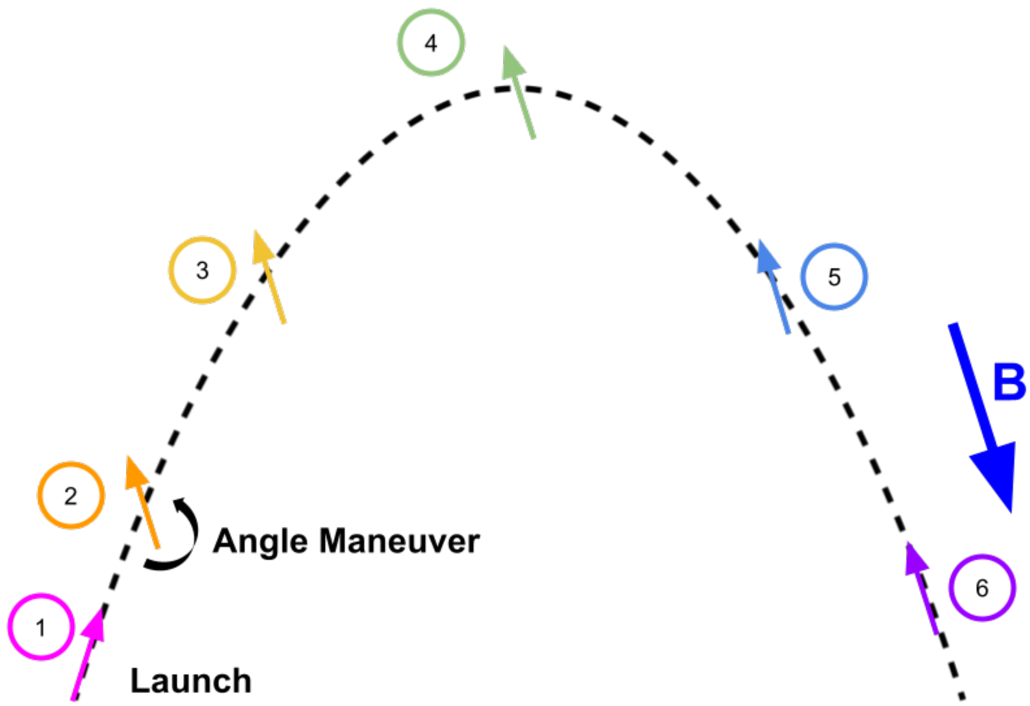

Figure 5.3: GNEISS rocket performs maneuver to align with magnetic field. Each rocket is launched with its long axes in line with its initial parabolic trajectory (1). Soon after, each rocket undergoes an angle maneuver (2), and maintains this attitude for the rest of the flight (3-6). This maneuver aligns the long axis of the rocket with the magnetic field shown in blue.

mission. A PIP tree is a simple structure to set a PIP at a certain elevation angle. On the forward deck, there is one PIP tree which houses the 30° and 75° PIPs and one that includes the 60° and 0° PIPs. On the aft deck, there is one PIP tree which houses the -30° and -90° PIPs and one that includes the -60° and 0° PIPs. The various PIP trees are shown in Figure 5.2. The trees are placed so that the PIPs are facing radially outward from the center of the sounding rocket. The trees will also have approximately 45° of separation on the deck (Figure 1.8). At a given moment, we will have two measurements for the ion flux through PIPs at two different clock angles on the deck. This separation allows us to solve for the ion flux direction and magnitude because we will have information about the component of ion flux in two nonparallel directions that are each perpendicular to the main axis of the rocket.

Each PIP tree is a thick block of aluminum mounted to the deck from the underside. The trees have large cross sections to prevent excessive deflection and vibration during flight while minimizing mass.

$$I = \frac{bh^3}{12} \tag{5.1}$$

$$\delta = \frac{FL^3}{3EI} \tag{5.2}$$

The greater base and height of the cross section contribute to a greater second moment of area, I, which will in turn decrease the maximum deflection, δ [14]. The PIP trees are made out of aluminum because it is a lightweight material that makes a smaller mass contribution given the increased volume.

The top of the blocks are machined to the desired elevation angle. These faces are sized to match the dimensions of the PIP base plate with corresponding tapped holes to mount the PIPs. The size of the faces was lengthened slightly to maintain adequate spacing between the gold planes of each of the two PIPs on the tree.

As of April 18th, 2025, the PIP trees are in their final design approval stages and will enter the manufacturing stage shortly.

5.2 Shield Board Boxes

Each pair of PIPs has a corresponding shield board, as shown in Figure 5.4. On the main payload, one shield board is paired with one tree, or pair, of PIPs. Each shield board needs to be housed to prevent damage and to keep it consistently oriented with the rocket.

Because there needs to be one shield board box for each pair of PIPs on the main payloads

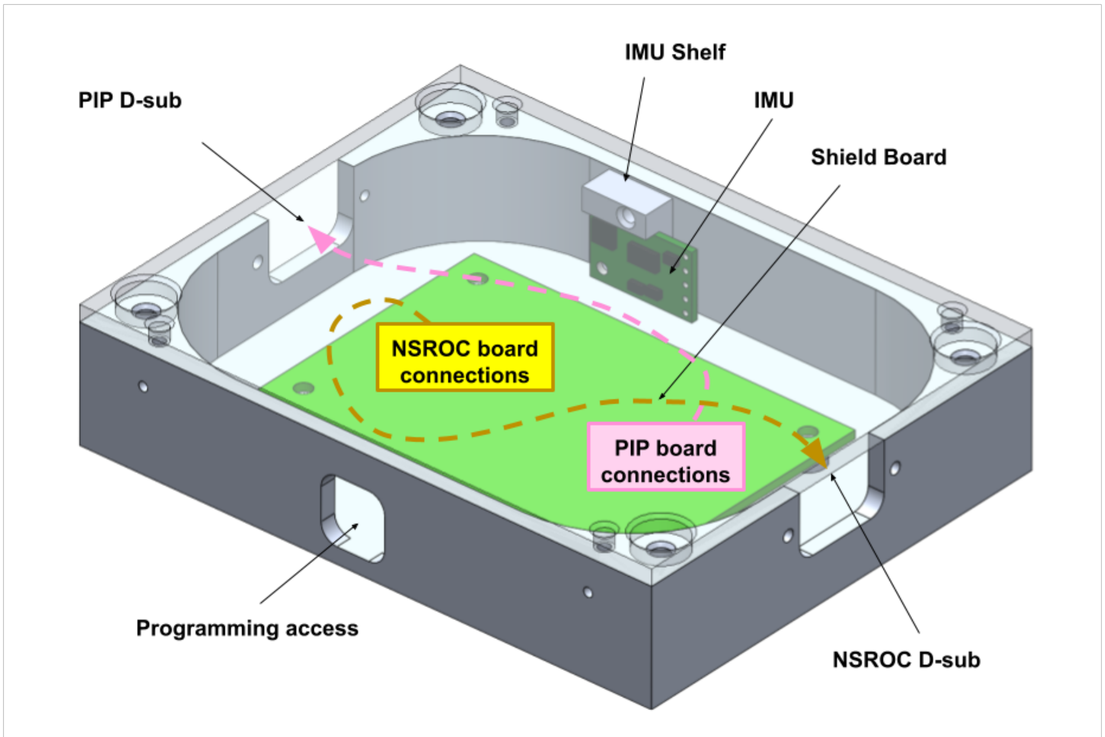

Figure 5.4: Shield board box. The box includes a shield board (in bright green) and an IMU (dark green). The shield board box lid is transparent in this figure to display the box's internal components. The box is 4.5" in length.

in addition to extras for bench testing and flight spares, we will make ten total boxes. This includes ten boxes, lids, and IMU shelves.

As mentioned in the Bob chapter, the shield board was designed by undergraduate students and a staff engineer in the 317 Rocket Lab. It is a 2" x 3" circuit board with 0.125" mounting holes at each of the corners. It includes a programming port at the center of one of the long sides. The shield board is also connected to an IMU. A shield board and an IMU are mounted to a machined shield board box in Figure 5.5.

The shield board box is a simple aluminum rectangle with a pocket deep enough to house the shield board and necessary wires. The shield boxes are made out of aluminum because it is a lightweight, relatively inexpensive, and easily machinable material. The pocket has heavily rounded corners to leave room in the corners for mounting holes and to decrease

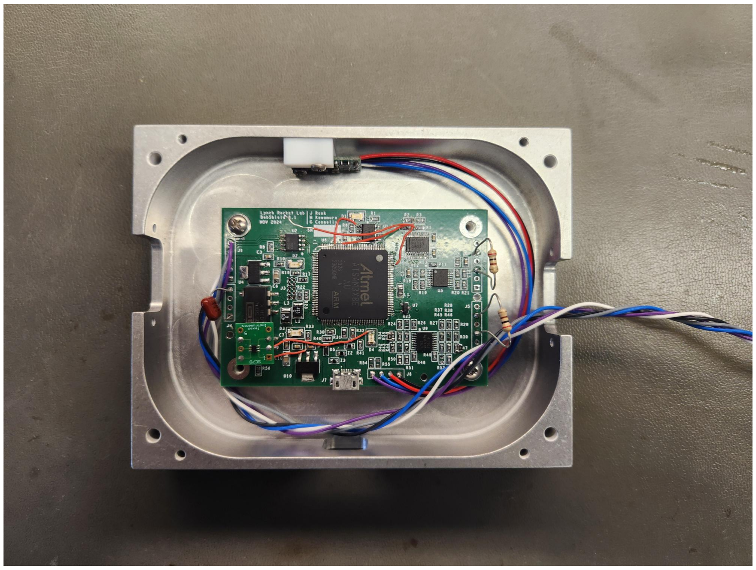

Figure 5.5: Machined shield board box with installed components and wiring. The shield board is mounted onto bosses located on the floor of the box. Photo courtesy of Jeffery Renk.

the number of tool changes while machining. There are four #4 clearance holes to secure the box to the deck and four additional #4-40 tapped mounting holes to secure the lid to the box. The tapped holes only extend 0.5" down into the volume of the box. This depth has sufficient thread engagement to secure the lid into place. These holes are vented at the bottom so air can escape out through the sides of the box. The bottom of the pocket has four identical bosses with tapped #4-40 holes to mount the shield board. The bosses are 0.125" tall to prevent the bottom side of the soldered PCB pads from being in electrical contact with the conductive aluminum box.

The lid is also a simple aluminum slab which matches the outer dimensions of the shield board box. It has #4 clearance holes so it can be mounted to the deck. The lid also includes #4 clearance holes with sufficient countersinks to mount the lid to the box. On the rocket, two of these boxes will be stacked and mounted together. It is important that the screws used to tighten the lid onto the bottom shield board box are below the plane of the lid because two of these boxes will be mounted in a stack on each deck.

The sides of the box each contain one important feature. One of the long edges of the shield board (the nearside in Figure 5.4) contains the programming port. I placed a 0.5" clearance square for easy programming access after the shield board box is assembled. Going clockwise, the next side of the box contains ports that need to be connected to the PIPs. The opposite side of the shield board contains ports that need to be connected to the NSROC side. I have included clearance holes and tapped mounting holes for two D-subs on the left and right walls of the box for the connections. A D-sub, or formally a D-subminiature, is a common electrical connector. The wires coming from each side of the shield board need sufficient space to bend. Therefore, the side of the shield board box which connects to the rocket, will make wire connections with the opposite side of the shield board, and vice versa for the PIP-side D-sub connector.

These D-subs will appear identical to the outside of the box. It is common practice for our lab to offset the D-sub that will connect with the PIP side of the electronics to differentiate the D-subs and prevent incorrect connections.

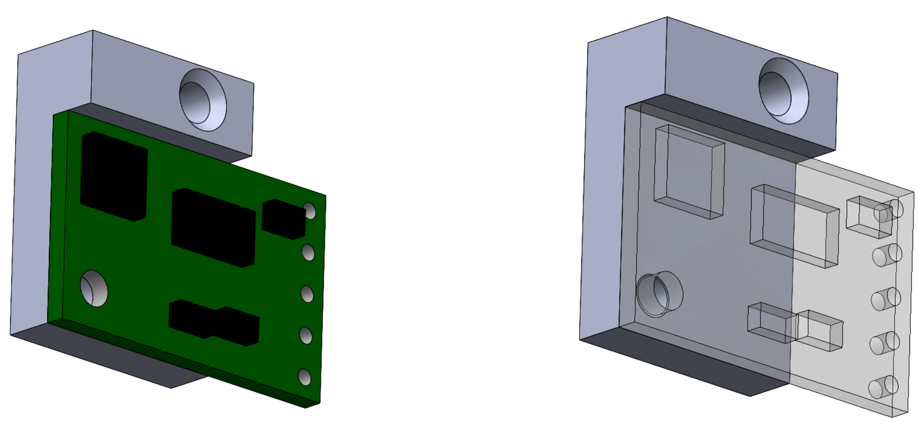

Figure 5.6: IMU shelf with IMU (left) and transparent IMU to show all features (right). The IMU Shelf electrically isolates the IMU from the aluminum shield board box while orienting to the axes of the box. In addition, the shelf provides clearance for wires soldered to the underside of the IMU. The IMU shelf is 0.5" wide.

The side opposite the programming port contains the IMU shelf, shown in Figure 5.6.

The IMU is used to identify the orientation of the shield box with respect to the Earth's magnetic field. It is important that the axes of the IMU exactly match the axes of the shield board box to correctly calibrate its orientation.

Each IMU has one #2 clearance hole for mounting, as shown in Figure 5.6. There are holes for soldering on the opposite side which need clearance underneath for wiring. I have made what I call an IMU shelf to locate the IMU while avoiding unwanted electrical connections. The shelf is made out of Teflon, a lightweight, non-conductive, and readily available material. The shelf allows one end of the IMU to hang off the edge which lets wires exit the soldered pads on the underside of the IMU and wrap around to connect with the main shield board. The shelf has one mounting hole for the IMU which only leaves one degree of freedom – rotation about the hole. There is a wall which the IMU makes contact with which prevents this rotation, completely constraining the IMU to the IMU shelf. The IMU shelf is mounted to the upper wall of the shield board box in two locations which completely constrains the IMU shelf and aligns it with the main axis of the shield board box. Both of the holes on the IMU shelf are #2 clearance holes for #2-56 screws.

As of April 15th, the shield board boxes have been machined and cleaned. Once the shield boards are fully tested and qualified, they will be mounted onto the boxes.

5.3 Lattice Box

In order to collect Lattice tomography data, we must emit an RF signal from each of the main payloads. This is done with an Ettus radio, a supporting Raspberry Pi, and a power amplifier. Each of these components are contained within a machined Lattice box that I have designed. Many of the design principles used to make this box are similar to the ones used to make the shield board box. Similarly to other components, the Lattice boxes are made of aluminum because it is a lightweight, relatively inexpensive, and easily machinable material.

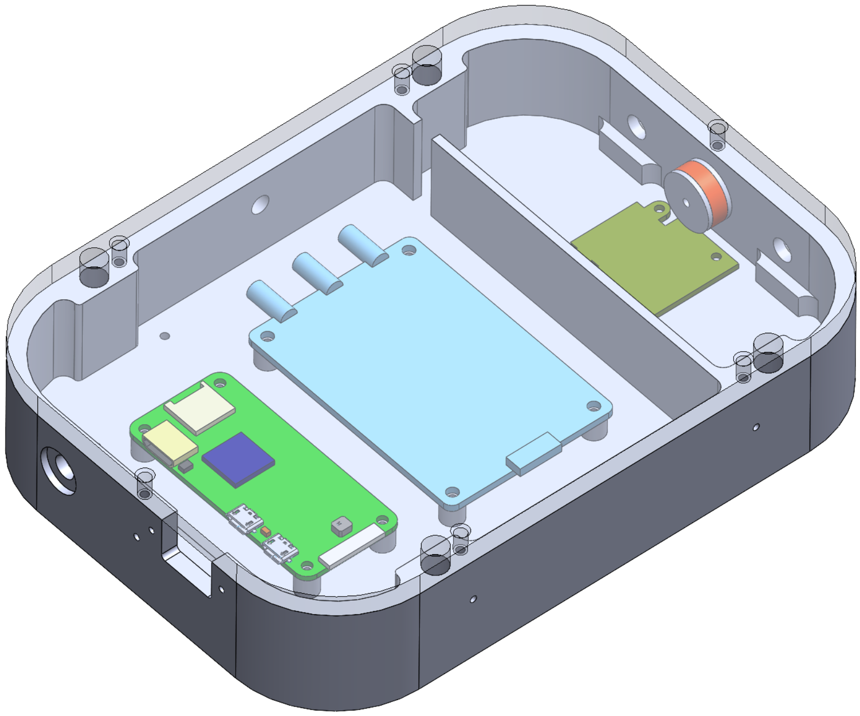

Figure 5.7: Lattice box with components. The Lattice box contains a Raspberry Pi (bright green), an Ettus radio (blue), a power amplifier (dark green), and a balun (red). The Lattice box lid has been made transparent in this model to feature the inner components. The Lattice box is 6” in length.

The Lattice box has a rectangular shape with sufficient pockets to properly house each of the essential components, as shown in Figure 5.7. The rectangular profile has heavily rounded corners because it had to snugly fit onto a spatially constrained deck for a preliminary test launch. The walls of the box are thin to minimize mass. Sections of the wall were thickened to make room for holes. Along the profile of the Lattice box, there are four $\#4-40$ mounting holes with deep counterbores to mount each box to the sounding rocket decks. There are also six tapped $\#4-40$ mounting holes to secure a simple aluminum lid of the same outer profile dimensions. The Lattice box lid is an aluminum rectangle which matches the outer dimensions of the Lattice box. The lid also includes six #4 clearance holes with sufficient countersinks to mount the lid to the box. It also has four clearance holes to provide access to the mounting holes in the Lattice box.

Power and input from one D-sub and one SMA cable control the Raspberry Pi and the Ettus radio. The Raspberry Pi communicates with the Ettus radio to send out an RF signal at a certain frequency. This signal is amplified by the power amplifier. This frequency is determined by NSROC for each flight to ensure that the frequency is unique for each rocket and different from any other receivable frequencies in the launch vicinity. The frequency is on the order of 150 MHz and is matched by the low-cost receivers distributed throughout rural Alaska.

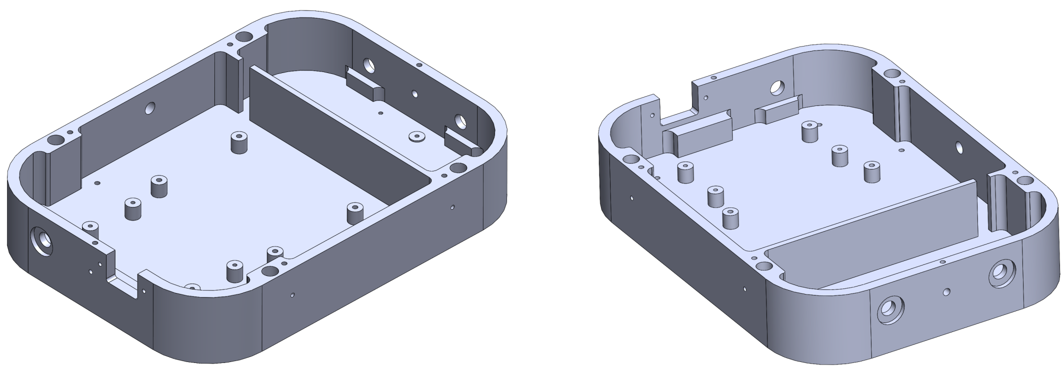

Figure 5.8: Lattice box without components at two viewing angles. The Lattice box features bosses, locations for high density D-sub and SMA connectors, anti-rotation steps, vents, a wall to contain the power amplifier, a place to mount a balun, and several tapped holes for tie-downs.

Within the rectangular box, each component is mounted to bosses which are machined directly in the box, as shown in Figure 5.8. The boss size and spacing corresponds to the size and spacing of each component's clearance holes. For example, the Raspberry Pi and the power amplifier use $\#2-56$ mounting screws while the Ettus radio uses $\#4-40$. The Raspberry Pi and Ettus radio bosses are 0.25" tall to allow room for components on their undersides while the power amplifier uses two 0.7 mm tall bosses to accommodate its unique geometry. The other two mounting locations for the power amplifier do not use bosses which allows it to make contact with the box and use it as a heat sink. There are also several $\#4-40$ tapped holes on the floor of the box for tie-downs. Many wires are traveling through this box and these tie-downs will help organize them. Each of these features is described in

Figure 5.9.

There is a 0.125" thick wall separating the section of the box housing the Ettus radio and Raspberry Pi and the section with the power amplifier. The wall has a small slit in it to allow for wires to travel through. This wall was added in later iterations of the box to have a low-cost, low-material way of partially thermally isolating the power amplifier from the rest of the components in the box. There is only one slit to let wires through to keep the wall as mechanically robust as possible. In previous iterations, there was a symmetrical slot on the opposite end of the wall as well. It was eliminated to prevent excessive vibration in the wall.

On the side of the box with the power amplifier, there are two SMA output holes (Figure 5.7. For these Lattice boxes, our lab has purchased off-the-shelf SMA connectors that bend at a 90° angle at one end to fit within the spatially minimized box. They are used to connect the Ettus radio to the input SMA in Figure 5.9 because the the Ettus radio ports are quite close to the Lattice box wall.

These connectors are secured to the Lattice box wall with an external nut. However, the connectors are not rotationally constrained to each of the connector holes in the box. This is an issue because the cable just spins inside the box when the nut is rotated in hopes of tightening it. To rotationally constrain them, I made anti-rotation steps, or elevated sections of the box, to make contact with the hexagonal collar on the SMA cable, which is coincident with the inner wall of the Lattice box, as shown in Figure 5.10. However, to further complicate the matter, the hexagonal collars are not at a constant angle relative to the 90° bend on the opposite end of the SMA cable. This is an issue because we need the freedom to direct the internal SMA cable in a specified direction to reach each internal SMA connection or over-bending the SMA cable. To account for this, I made the elevated sections a certain height to allow for no more than 60° of rotation for any given SMA cable. This gives us enough freedom to direct the internal cable while not allowing it to rotate freely, allowing the nut to be tightened. There is also an anti-rotation step below the input SMA.

Both locations are shown in Figure 5.9.

In addition to the anti-rotation steps, there are two anti-vibration supports along the perimeter of the Lattice box inner pocket, as shown in Figure 5.9. Both the Raspberry Pi and the Ettus radio have micro-USB ports. Because of the limited space for connectors, we used 90° micro-USB boards which serve as an adapter between the micro-USB ports and the individual wires that exit the input D-sub. Simply plugging in the micro-USB board into the micro-USB ports, however, does not sufficiently secure the micro-USB ports into place. This becomes an issue especially in high-vibration environments, such as a sounding rocket during launch. To compensate for this, anti-vibration supports were added to press against the back of the micro-USB boards. When these boards vibrate during the mission, the supports will ensure that they do not lose electrical connection.

In between the SMA cable holes on the power amplifier side of the box is a mounting hole for a balun bobbin clamp, as shown in Figure 5.11. Baluns are electrical components in radios used to balance the impedance. Our balun is a compact toroid coil. We will mount the balun with two Teflon bobbin clamps that will keep the balun electrically isolated from the box. Similar to a bobbin in a sewing machine, the clamp has two thin discs with a small cylinder connecting two. I have cut the traditional sewing machine bobbin shape in half to use it as a clamping mechanism for the toroid balun. The bobbin clamp half closer to the wall has a clearance hole while the bobbin clamp farther from the wall has a threaded hole, similar to a nut. A $\#4 - 40$ screw is used to secure the balun and the clamping piece in place, which will be inserted through the #4 clearance hole in the Lattice box wall.

As of April 15th, 2025, the final Lattice box design has been delivered to our machinists. Once they are machined, they will be cleaned. After that, the components will be mounted to the box. Finally, the Lattice box will undergo testing.

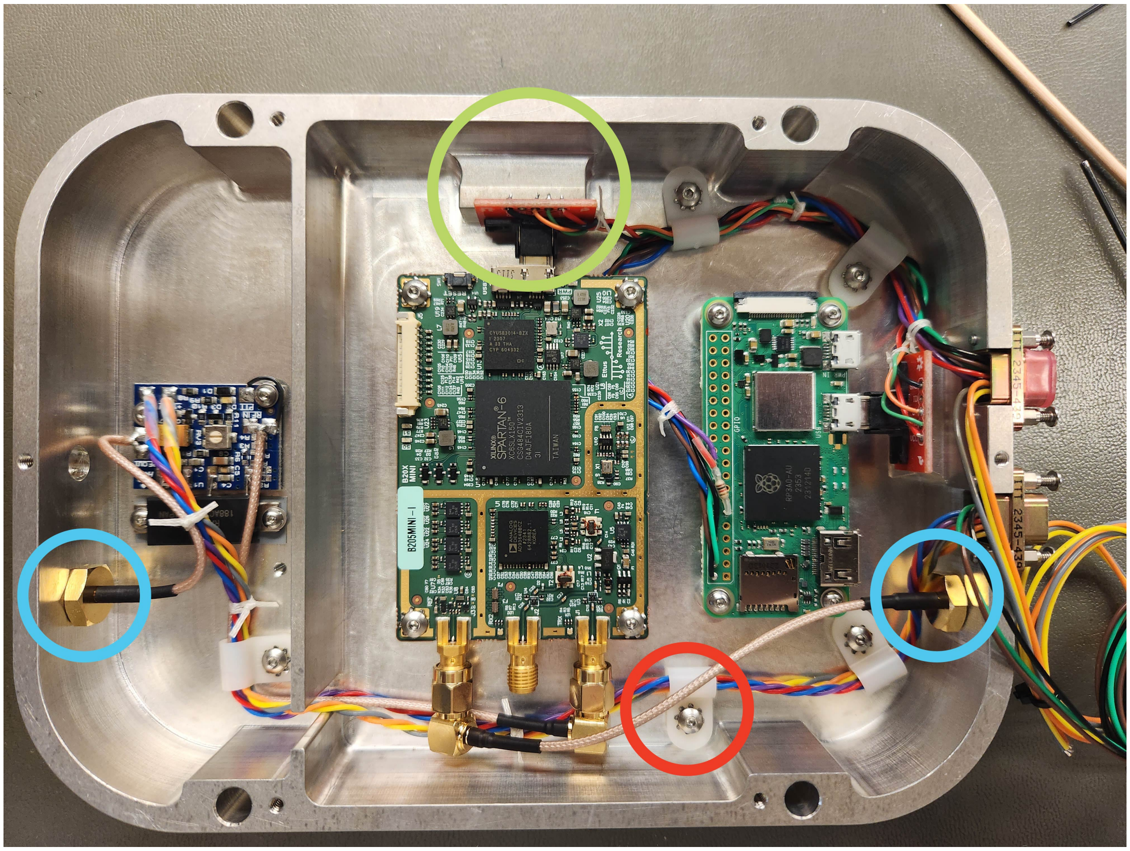

Figure 5.9: Previous iteration of Lattice box featuring SMA cables, tie-downs, and anti-vibration supports. The hexagonal collars of the SMA cables are circled in blue. The lack of anti-rotation steps allows the cables to freely rotate when they are fastened in the clearance holes in the Lattice box wall. One of the tie-down clamps is circled in red. There are several of these throughout the box to organize wires. One of the anti-vibration supports is circled in green. These help stabilize the boards inserted into the micro-USB ports in high-vibration environments. Note that this is a previous iteration of the Lattice box. The most current design has an additional SMA cable near the power amplifier (left side). Photo courtesy of Jeffery Renk.

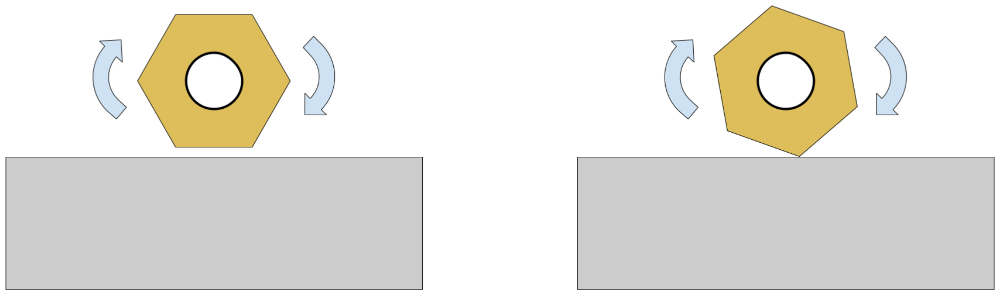

Figure 5.10: Anti-rotation steps prevent the SMA hexagonal collars from rotating more than 60°. When a flat side of the hexagonal collar is parallel to the step, the SMA cable has some freedom to rotate in either direction (left). Once the SMA has rotated just under approximately 60°, the high point on the collar will make contact with the anti-rotation step to prevent additional rotation in that direction (right).

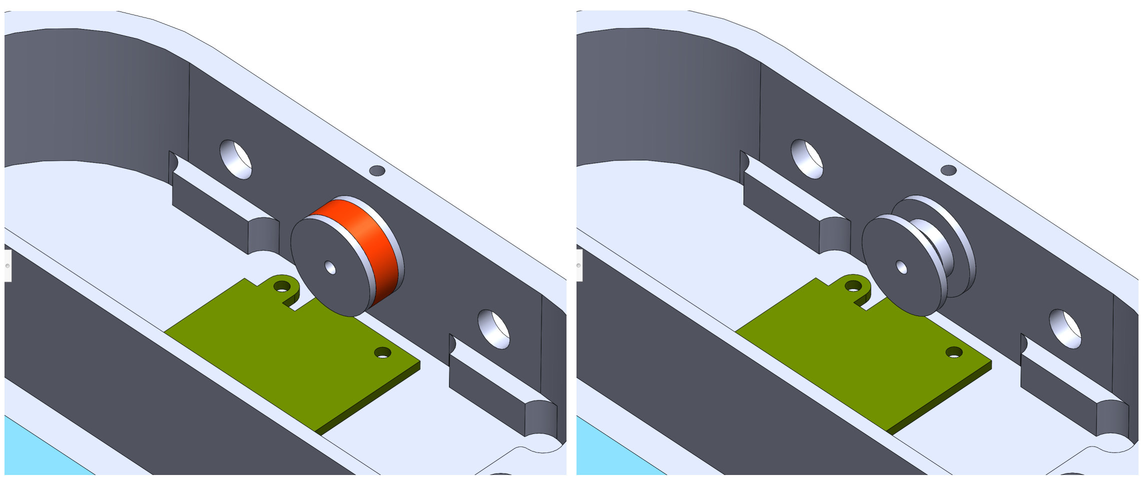

Figure 5.11: Balun bobbin clamp with toroid balun (left) and without balun to show all features (right). The bobbin clamp allows the balun to be easily mounted to the Lattice box wall while being electrically isolated. The threaded bobbin clamp is on the left side of the unthreaded bobbin clamp.

Chapter 6

Next Steps

Over the course of my thesis project, I successfully designed and improved a family of flight hardware for the GNEISS rocket mission. I devised a new method to secure the PIP screens which prompted a new mechanical design and allowed for a more efficient fabrication process. I was able to decrease the labor time for the PIP fabrication process by 75% while maintaining the same electrical function. By expediting this process, our lab can reallocate our time to improving other processes or iterating other designs.

Another major improvement I made was the assembly process for the Bob given the constraint of including one side PIP and one forward PIP. With this improvement, I ultimately decreased the time of assembly by 50%. With the challenge of integrating multiple inherent mass asymmetries, I simultaneously improved the inertia tensor to a nearly diagonalized state and decreased the total mass of the Bob to achieve improved flight parameters.

6.1 Next Steps

Due to the timeline of sounding rocket missions, design iterations will continue over the upcoming months leading up to the integration stage in October and November of this year. Until then, several teams at Dartmouth and NSROC will finalize designs and complete tests to qualify the flight hardware.

As of April 2025, all mechanical designs have been approved for manufacturing. Once each hardware element has been machined, cleaned, and properly assembled, the electrical components must be tested. Currently, undergraduates and our staff engineer are working to test the electrical connections on the preamp board, which is installed onto each of the PIPs. Similar tests must be performed with the electronics on the Bobs, shield board boxes, and Lattice boxes.

Once the hardware pass electrical testing, they will each undergo testing in our plasma chamber. The chamber simulates the plasma environment, which the GNEISS sounding rockets will fly through, to qualify the PIPs' function. In addition, one of each hardware element will be sent to NASA's Wallops Flight Facility to undergo vibration testing. This is especially important for the PIP trees, shield board boxes, and Lattice boxes which are brand new designs that do not have a heritage of previous vibration tests.

If all of the hardware elements are qualified for flight, we will begin the first round of system-level testing. For example, we will mount the PIPs to the PIP trees and connect them to a corresponding shield board box then repeat the same tests described above. At this stage, we will also test the hardware in a vacuum for three consecutive flight durations to confirm that they do not overheat in a vacuum environment absent of convective cooling.

After the first round of system-level tests are complete, it is time for integration. The sounding rockets will be assembled at NASA's Wallops Flight Facility in Virginia. All hardware will be mounted onto the sounding rockets for complete system-level testing. This includes tests that simulate the sounding rocket's environment. The hardware will undergo a shake test to simulate a turbulent launch. The sounding rocket structures will undergo a bend test in which the tip of the rocket (the nose) will be pulled to the side to qualify the strength of the rocket structure. All RF systems will be tested to confirm that they can complete their tasks simultaneously without interference. Finally, all electronics will be tested to confirm that all data acquisition commands are successful.

The sounding rockets will be shipped in segments to Alaska in early 2026. The rockets will be reassembled on arrival and prepared for launch. The final tasks include removing protective plastic covers on the PIPs and anything else on the remove-before-flight list.

In March 2026, we will ready the rockets and wait for the perfect aurora.

6.2 Continuing Work on the GNEISS Mission

When I return to Dartmouth in the fall as a fifth-year dual degree student, I will continue my work in the 317 Lab. In the fall, I will make any necessary revisions prompted by the qualification tests performed over the summer. In addition, I will reassume the project manager role for GNEISS hardware manufacturing and fabrication. In this role, I will continue to plan and track all manufacturing and fabrication tasks and timelines. In addition, I will create and maintain an organized archive of all mechanical designs from the GNEISS mission to inform future sounding rocket mission hardware created by the 317 Lab.

Appendix A

Hardware Quantities

Table A.1: Hardware quantities categorized by flight part, flight spare, and bench.

Item	Flight	Flight Spare	Bench	Total
PIPs	24	4	4	32
Screen sets	24	4	4	32
Screen covers	24	4	4	32
Main Payload Gold Planes	16	2	1	19
Bobs	4	1	1	6
Bob Forward Gold Planes	4	1	1	6
Bob Side Gold Planes	4	1	1	6
Shield Board Boxes	8	1	1	10
Lattice Boxes	2	1	1	4
PIP Trees ($75°$ & $30°$)	2	0	0	2
PIP Trees ($90°$ & $30°$)	2	0	0	2
PIP Trees ($60°$ & $0°$)	4	0	0	4

Appendix B

SolidWorks

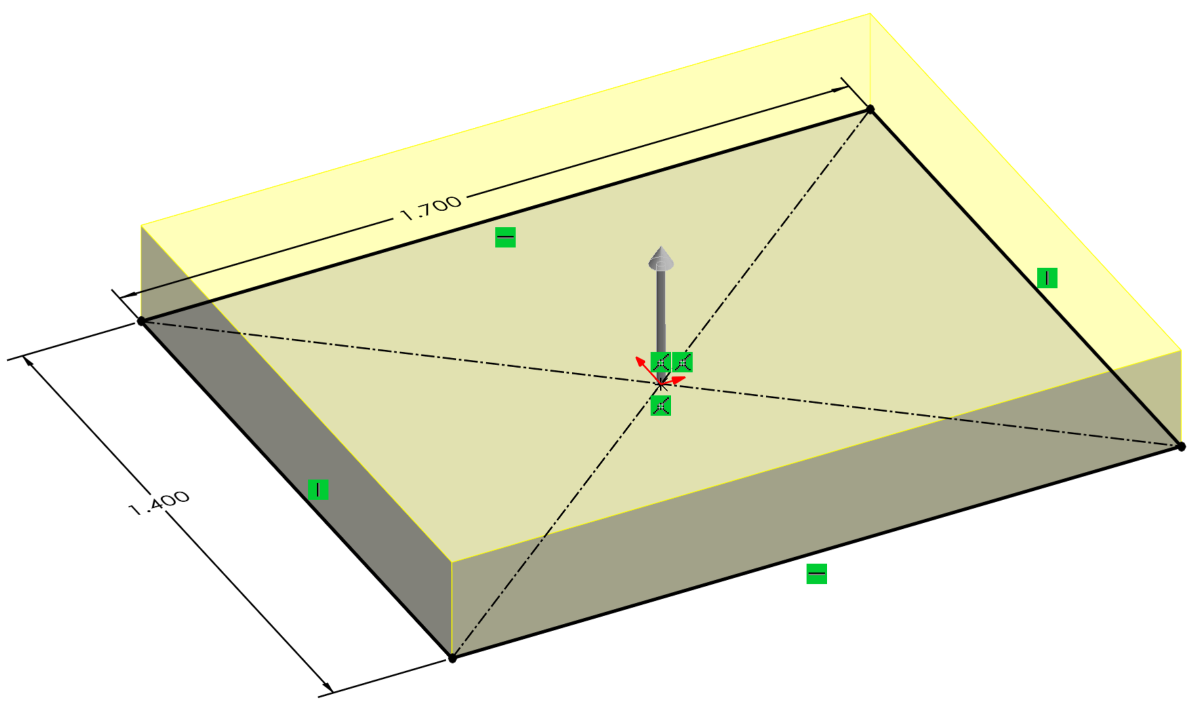

Figure B.1: SolidWorks 2D sketch and extrude feature. This dimensioned 2D sketch was used to create the base geometry for the PIP top housing.

I used SolidWorks 2024, a CAD (computer-aided design) software, to design each of the parts and assemblies created for this thesis project. SolidWorks allows you to create 2D sketches with a defined geometry. If a 2D sketch includes a closed shape, it can be extruded to create a 3D volume, called a body. This was done to create the base geometry for the PIP housing top as seen in Figure B.1. An extrusion is a type of feature. Once a body exists, other features, such as extruded cuts, holes, and fillets, can be applied to the body. This defined 3D body is the geometry for a single part.

Once a part is designed in SolidWorks, it can be added to an assembly. In SolidWorks terms, an assembly is a group of parts with defined spatial relationships. By creating assemblies in SolidWorks, complex mechanical hardware, such as the PIPs and Bobs, can be easily visualized and measured.

SolidWorks is also able to make mass calculations. When the material for a part is specified, it uses the geometry and density to deliver mass properties, such as total mass, center of mass, and the inertia tensor. This was especially helpful when calculating the inertia tensor for the Bob. Because SolidWorks was able to quickly deliver an accurate inertia tensor, I could efficiently iterate the Bobs.

Appendix C

Project Management

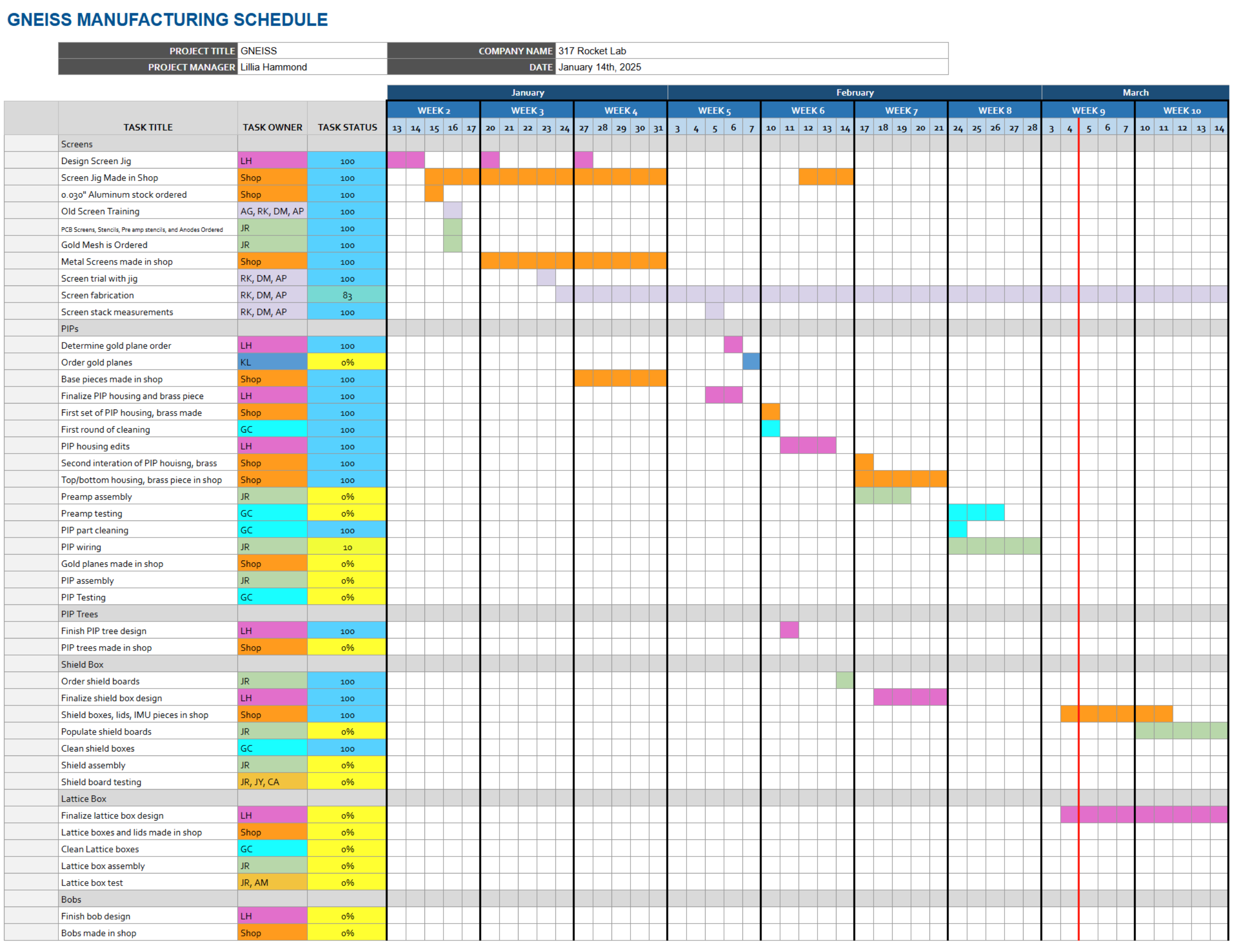

Figure C.1: Winter Gantt chart describing manufacturing tasks, timing, and responsibilities.

During Dartmouth's 2025 Winter quarter, I served as the primary project manager for Dartmouth-based manufacturing and fabrication processes within the GNEISS mission. My responsibilities included developing a detailed schedule of all manufacturing tasks to meet a target end date, managing lead times for stock material and commercially purchased parts, and maintaining lines of communication among multiple manufacturing and fabrication subgroups, machinists, and engineers at NSROC.

Appendix D

Gold Plane Optimization

The gold plane stock material is especially expensive. In order to minimize costs, we have to survey multiple suppliers to find the best price. In the past, we have ordered precut circular planes. For this mission, we are considering purchasing rectangular gold sheets which we would cut ourselves. The precut features adds labor costs up front, but by purchasing the rectangular gold sheet stock, we are also paying for the wasted gold material in between the circular cutouts.

Our lab is considering purchasing rectangular gold sheet stock material from a supplier in 4” by 36” sheets. My task was to calculate how many 2.25” main payload gold planes we could cut from one sheet of this stock material.

In this classic geometric brain-teaser, I began by fitting one circle in the corner of the stock sheet, tangent to the left and bottom edges as seen in Figure D.1. Then, I fit a second circle tangent to the first circle and top edge of the stock. The next circle is fit tangent to the second circle and the bottom edge of the stock and so on until the whole stock is used.

I will first inspect the distance between the center of the first two circles. I can take advantage of tangencies to determine the distance from the first circle’s center to each edge is r, the radius of the main payload gold plane which is 1.125”. Similarly, I can infer that the vertical distance from the second circle to the top edge of the stock is also r. Given that the

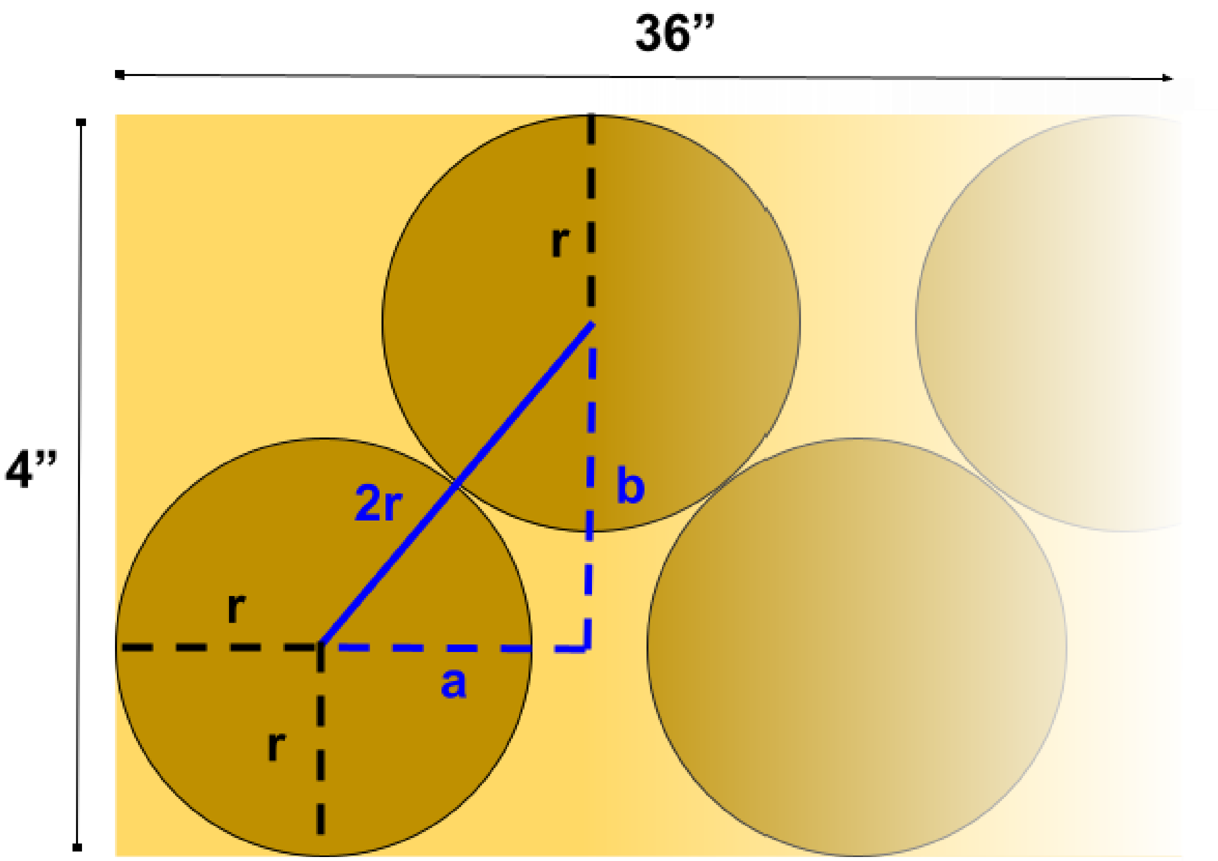

Figure D.1: Gold plane optimization. Geometric exercise to determine how many 2.25” main payload gold planes can fit within a 4” by 36” rectangular sheet of gold plane stock material. Each circular gold plane is tangent to the edges of the stock and its adjacent circular gold planes.

stock is 4” in width, I can determine that the vertical distance between the first two circles' centers, b in Figure D.1, is 1.75”.

I also know that the distance between the two circles' centers is $2r$ because the circles are tangent to each other. Using the Pythagorean Theorem, I can solve for the horizontal distance between the first two circles, a in Figure D.1.

$$a = \sqrt{(2r)^2 - (b)^2} \tag{D.1}$$

This delivers 1.414" as the horizontal distance between the first two circles. Due to the uniform width of the stock material and diameter of the main payload gold planes, this will also be the horizontal distance between every pair of adjacent circles. Therefore, the horizontal length of the packed circles will be $1.414(n-1)+2.25$ where n is the number of circles.

I am trying to fit as many circles as possible into the 36" stock length, which is represented by

$$36 > 1.414(n-1)+2.25 \tag{D.2}$$

which delivers

$$n < 24.86. \tag{D.3}$$

Because n must be an integer, the maximum number of main payload gold planes that can be made from this sheet of stock is 24. This amount will inform our supplier selection process.

Bibliography

[1] "What Is the Solar Wind?" URL https://science.nasa.gov/sun/what-is-the-solar-wind/.

[2] D. J. Griffiths, *Introduction to Electrodynamics* (Cambridge University Press, Shaftesbury Road, Cambridge CB2 8EA, United Kingdom, 2024).

[3] M. C. Kelley, "Chapter 1 - Introductory and Background Material," in "The Earth's Ionosphere," , edited by M. C. Kelley (Academic Press, 1989), pp. 1–22, ISBN 978-0-12-404013-7, URL https://www.sciencedirect.com/science/article/pii/B978012404013750006X.

[4] "Aurora Tutorial," URL https://www.swpc.noaa.gov/content/aurora-tutorial.

[5] H. Frey, D. Han, R. Kataoka, and et al, "Dayside Aurora," Space Science Review **215** (2019), URL https://link.springer.com/article/10.1007/s11214-019-0617-7#citeas.

[6] K. Lynch, personal communication.

[7] D. M. Gillies, D. J. Knudsen, E. F. Donovan, E. L. Spanswick, C. Hansen, D. Keating, and S. Erion, "A survey of quiet auroral arc orientation and the effects of the interplanetary magnetic field," Advancing Earth and Space Sciences **119** (2014), https://agupubs.onlinelibrary.wiley.com/doi/full/10.1002/2013JA019469, URL https://doi.org/10.1002/2013JA019469.

[8] C. Gasque, Presentation at a Symposium.

[9] S. Christe, B. Zeiger, R. Pfaff, and M. Garcia, "Introduction to the Special Issue on Sounding Rockets and Instrumentation," Journal of Astronomical Instrumentation **5** (2016), URL https://www.worldscientific.com/doi/abs/10.1142/S2251171716020013.

[10] J. Adkins, "About Sounding Rockets," (2023), URL https://www.nasa.gov/soundingrockets/overview/.

[11] M. Fraunberger, K. A. Lynch, R. Clayton, T. M. Roberts, D. Hysell, M. Lessard, A. Reimer, and R. Varney, "Auroral ionospheric plasma flow extraction using subsonic retarding potential analyzers," Review of Scientific Instruments **91**, 094503 (2020), ISSN 0034-6748, https://pubs.aip.org/aip/rsi/article-pdf/doi/10.1063/1.5144498/14800429/094503_1_online.pdf, URL https://doi.org/10.1063/1.5144498.

[12] T. M. Roberts, K. A. Lynch, R. E. Clayton, J. Weiss, and D. L. Hampton, "A small spacecraft for multipoint measurement of ionospheric plasma," Review of Scientific Instruments **88**, 073507 (2017), ISSN 0034-6748, https://pubs.aip.org/aip/rsi/article-pdf/doi/10.1063/1.4992022/14787703/073507_1_online.pdf, URL https://doi.org/10.1063/1.4992022.

[13] R. H. Burth, P. G. Cathell, D. B. Edwards, A. H. Ghalib, J. C. Gsell, H. C. Hales, H. C. Haugh, and B. R. Tibbetts, "NASA sounding rockets user handbook," (2023), URL https://sites.wff.nasa.gov/code810/files/SRHB.pdf.

[14] L. Hammond, Class Notes from ENGS 33: Solid Mechanics at Dartmouth College Thayer School of Engineering with Prof. Douglas Van Citters.

[15] T. M. Roberts, K. A. Lynch, R. E. Clayton, M. E. Disbrow, and C. Hansen, "Magnetometer-Based Attitude Determination for Deployed Spin-Stabilized Space-

craft," Aerospace Research Central **40** (2017), https://arc.aiaa.org/doi/10.2514/1.G002591, URL https://doi.org/10.2514/1.G002591.

[16] K. Lynch, personal communication.

[17] J. R. Taylor, *Classical Mechanics* (University Science Books, Mill Valley, California, 2005).